A study of the ground and excited states of Al$_3$ and Al$_3^-$. II. Computational analysis of the 488 nm anion photoelectron spectrum and a reconsideration of the Al$_3$ bond dissociation energy

Stephen R. Miller,[a] Nathan E. Schultz,[b] Donald G. Truhlar,[c] and Doreen G. Leopold[d]
*Chemistry Department, University of Minnesota, 207 Pleasant Street S.E., Minneapolis,
Minnesota 55455, USA*

Computational results are reported for the ground and low-lying excited electronic states of Al$_3^-$ and Al$_3$ and compared with the available spectroscopic data. In agreement with previous assignments, the six photodetachment transitions observed in the vibrationally resolved 488 nm photoelectron spectrum of Al$_3^-$ are assigned as arising from the ground $\widetilde{X}\,^1A_1'(^1A_1)$ and excited $^3B_2$ states of Al$_3^-$ and accessing the ground $\widetilde{X}\,^2A_1'(^2A_1)$ and excited $^2A_2''(^2B_1)$, $^4A_2$, and $^2B_2$ states of Al$_3$ (with C_{2v} labels for D_{3h} states in parentheses). Geometries and vibrational frequencies obtained by PBE0 hybrid density functional calculations using the 6-311+G(3d2f) basis set and energies calculated using coupled cluster theory with single and double excitations and a quasiperturbative treatment of connected triple excitations (CCSD(T)) with the aug-cc-pVxZ {x=D, T, Q} basis sets with exponential extrapolation to the complete basis set limit are in good agreement with experiment. Franck–Condon spectra calculated in the harmonic approximation, using either the Sharp–Rosenstock–Chen method which includes Duschinsky rotation or the parallel-mode Hutchisson method, also agree well with the observed spectra. Possible assignments for the higher-energy bands observed in the previously reported UV photoelectron spectra are suggested. Descriptions of the photodetachment transition between the Al$_3^-$ and Al$_3$ ground states in terms of natural bond order (NBO) analyses and total electron density difference distributions are discussed. A reinterpretation of the vibrational structure in the resonant two-photon ionization spectrum of Al$_3$ is proposed, which supports its original assignment as arising from the $\widetilde{X}\,^2A_1'$ ground state, giving an Al$_3$ bond dissociation energy, $D_0(\text{Al}_2-\text{Al})$, of 2.403 ± 0.001 eV. With this reduction by 0.3 eV from the currently recommended value, the present calculated dissociation energies of Al$_3$, Al$_3^-$, and Al$_3^+$ are consistent with the experimental data. © *2009 American Institute of Physics.*
[DOI: 10.1063/1.3008056]

I. INTRODUCTION

Small aluminum clusters provide a topic accessible to a variety of spectroscopic and computational approaches, enabling the insights gained by each method to check and elucidate the others. While simple enough to be characterized by both wave function theory[1–14] and density functional theory (DFT),[15–21] small aluminum clusters also share some properties in common with the more electronically complex transition metal clusters. These include the ability to form both σ- and π-type bonds and the presence of low-energy electronic states with different spin multiplicities. The spectroscopy and reactivity of both types of metal clusters are also enriched by the potentially multivalent character of the bonding, which may involve both 3p and 3s atomic character for Al, or ns and $(n-1)d$ character for transition metals.

Thus, results for these simpler p-block metal clusters are useful complements to studies of the less computationally tractable d-block metal clusters.

Spectroscopic and computational studies of small metal clusters have, in addition to their fundamental interest, the broader potential impact of contributing to the development of approximate computational methods capable of predicting the properties of metal catalysts and other technologically important materials incorporating metal nanoparticles. Although this point is often used to motivate the study of clusters, aluminum clusters provide one of the few examples of metallic systems in which this bootstrapping approach has actually been successfully applied to predict size-dependent properties over the entire range of size scales.[22–33] In this series of studies, two of us (N.E.S. and D.G.T.) and our collaborators have used high-level *ab initio* wave function theory to predict the geometries, dissociation energies, and other properties of angstro-scale Al$_n$ aluminum clusters (n =2–7).[22] These computational results were used to test DFT methods employing all-electron basis sets, which were applied to larger metal clusters ($n \leq 13$). These results were then added to the database, which served to validate DFT

---
[a] Present address: Department of Chemistry, Gustavus Adolphus College, 800 W. College Ave., St. Peter, MN 56082.
[b] Present address: 3M Corporate Research Laboratory, 3M Center, Bldg. 0201-03-E-23, St. Paul, MN 55144-1000.
[c] Electronic mail: truhlar@umn.edu.
[d] Electronic mail: dleopold@umn.edu.

methods employing a valence electron basis set combined with an effective core potential,[25] and this more economical method was applied to yet larger nanoscale particles (up to $n = 177$, which is a 2 nm particle). Finally, an expanded training set, incorporating this computational nano-Al database as well as experimental data for the face-centered cubic crystal phase and theoretical data for other crystal habits, was used to develop accurate analytical potential energy functions applicable to the macroscopic scale.[26,33] These potential functions have been employed to predict the thermodynamic properties of aluminum nanoparticles[31–33] and the phase behavior of elemental aluminum.[27,28] This series of studies was motivated by the need for computational methods capable of predicting size-dependent properties,[33,34] such as melting points, which are important for the further development of technological processes employing aluminum particles, for example as solid rocket propellants.

In this systematic, atom-up computational strategy, the aluminum trimer provided one of the smallest and thus most foundational components. We focus here on a comparison of computational predictions for Al_3 and Al_3^- with experimental measurements from the vibrationally resolved 488 nm (2.540 eV) anion photoelectron spectrum of mass-selected Al_3^- reported in the preceding paper,[35] which we will call "Paper I," and from other spectroscopic studies.[36–42] Calculations reported here for the equilibrium geometries and vibrational frequencies of the Al_3 and Al_3^- ground and excited electronic states employ PBE0 hybrid DFT with an all-electron basis set, and energies are calculated by the CCSD(T)/CBS (complete basis set) coupled cluster (CC) method. Based on these computational results, harmonic Franck–Condon simulations of the photoelectron spectra are generated to test the state assignments proposed in Paper I and to further assess the accuracy of these computational techniques as applied to the ground and excited electronic states of Al_3 and Al_3^-.

In the database developed for the aluminum cluster and nanoparticle calculations, the primary property used for fitting was the geometry-dependent atomization energy.[33] Thus, it is a concern that the Al_3 atomization energy of 3.76 eV (86.7 kcal/mol) predicted in previous computational studies[4] using state-of-the-art wave function theory that is expected to be accurate is 0.28 eV (6.5 kcal/mol) lower than the 4.04 ± 0.07 eV value obtained from the experimentally measured $D_0(Al_2 - Al)$ (Ref. 38 and 39) and $D_0(Al_2)$ (Ref. 43) dissociation energies. The former value, obtained from the resonant two-photon ionization (R2PI) spectrum of Al_3,[38] had been incremented by 0.30 eV in view of the assignment of the initial electronic state probed in this experiment as the excited $^4A_2$ state lying 0.30 eV above the ground state.[39] The conflict between experiment and theory for the Al_3 dissociation energy suggests a return to the original assignment of the R2PI spectrum as arising from the Al_3 ground state,[38] and a reinterpretation of the R2PI vibrational structure consistent with this assignment is suggested here.

This manuscript is organized as follows. First, the computational methods used to calculate the ground and excited state properties of Al_3 and Al_3^- and to generate the simulated Franck–Condon spectra are described. The computational re-

sults are then presented and compared with the 488 nm (Ref. 35) and UV (Ref. 36 and 37) anion photoelectron spectra and with the experimental bond dissociation energy data.[38,39] The R2PI spectrum[38] of Al_3 is then described and its proposed reassignment is discussed. The different Franck–Condon analysis methods employed in the present set of papers are compared. The transition between the Al_3^- and Al_3 ground states is elucidated through the use of total electron density difference distributions. The final section summarizes the key conclusions.

II. COMPUTATIONAL METHODS

II.A. Electronic structure

The geometry optimizations and harmonic vibrational frequency calculations reported here were performed using the GAUSSIAN software package[44] by self-consistent field (SCF) calculations with the PBE0 hybrid density functional[45,46] and the all-electron 6-311+G(3d2f) basis set.[47] This basis set, in which three d and two f functions are added for each nonhydrogenic atom, is equivalent for Al to the MG3 (Ref. 22) basis set. The PBE0 method (which is specified in GAUSSIAN as PBE1PBE, also known as PBEh) retains 100% of the PBE correlation functional but replaces 25% of the PBE exchange functional by Hartree–Fock exchange.[45,46] This combination of functional and basis set, PBE0/MG3, was found in previous studies to be the most reliable for calculations of small Al-containing molecules among several density functionals and basis sets tested.[22] "Tight" criteria were used for wave function convergence and geometry optimization, and frequency calculations employed ultrafine integration grids. For compatibility with the Franck–Condon analysis program described below, the frequency calculations were run separately and the *iop* (7/33 =1) keyword (which provides high precision in the normal mode Cartesian displacements) was included. Electron density plots were prepared with GAUSSVIEW 4.1.

Electronic state energies of Al_3 and Al_3^- were also calculated at the PBE0 equilibrium geometries using the CCSD(T) open-shell, single-reference coupled-cluster (CC) correlation method with single and double excitations and a quasiperturbative treatment of connected triple excitations,[48] as implemented in the MOLPRO software package.[49] The CC method employed here [MOLPRO acronym UCCSD(T)] uses a high-spin restricted Hartree-Fock (RHF) reference wave function.[50] The CC calculations employed the augmented, correlation-consistent, polarized valence aug-cc-pVxZ, x ={D,T,Q} double, triple, and quadruple ζ quality basis sets.[51] Calculated energies were extrapolated to the complete basis set (CBS) limit using the following function, where n =2, 3, and 4 for the DZ, TZ, and QZ basis sets, respectively,[4,6]

$$E_{(n)} = E_{CBS} + A \exp[-(n-1)] + B \exp[-(n-1)^2]. \quad (1)$$

Parameters E_{CBS}, A, and B were adjusted using the EXCEL solver tool to give the minimum value (typically $\sim 10^{-10}$) for the sum of the squares of the differences between the three $E_{(n)}$ values and the total calculated energies obtained with the corresponding basis sets. For brevity, this

CCSD(T)/CBS//PBE0/MG3 method is simply referred to below as the "CC" method. The resulting energy of each excited electronic state of Al_3 or Al_3^-, relative to the ground state energy, was converted using its harmonic PBE0 zero point vibrational energy to obtain the T_0 energies and adiabatic electron affinities reported here, for direct comparison with the spectroscopic results.

II.B. Franck–Condon simulations

Franck–Condon simulations of the vibrational structure associated with each photodetachment transition $(Al_3 + e^- \leftarrow Al_3^-)$ were calculated in the harmonic approximation using the programs FCFGAUS and PESCAL by Ervin, Lineberger, and co-workers.[52–55] FCFGAUS extracts the required information directly from the output files of the PBE0 GAUSSIAN frequency jobs for the Al_3 and Al_3^- states. The values used are the calculated equilibrium geometry, the atomic mass ($m_{Al} = 26.981\,54$ amu), and, for each of the three normal modes of a triangular structure, its vibrational frequency, Cartesian atomic displacements, and reduced mass (which, in this case, is simply m_{Al}). From these predictions, the $\mathbf{J}$ (Duschinsky normal mode rotation) matrix and $\mathbf{K}$ (normal mode displacement) vectors are calculated following the method introduced by Chen and co-workers.[56,57] Based on this information, PESCAL calculates Franck–Condon factors for individual vibronic transitions using the generating function method of Sharp and Rosenstock.[58] These calculations include hot and sequence bands arising from the excited vibrational levels of the anion. This method of calculating polyatomic Franck–Condon factors in the harmonic approximation, including Duschinsky rotation, by using the algorithms of Sharp, Rosenstock, and Chen, is referred to below as the "SRC method."

The normal coordinates of the initial anion state $(\mathbf{Q}'')$ can be expressed in terms of those of the final state of the neutral molecule $(\mathbf{Q}')$,

$$\mathbf{Q}'' = \mathbf{J}''\mathbf{Q}' + \mathbf{K}''. \tag{2}$$

For the present case of a homonuclear triatomic, $\mathbf{J}''$ and $\mathbf{K}''$ simplify as follows:

$$\mathbf{J}'' = (\mathbf{N}'')^T\mathbf{N}' \quad \text{(unitless)}, \tag{3}$$

$$\mathbf{K}'' = \sqrt{m}(\mathbf{N}'')^T\mathbf{R} \quad (\text{amu}^{1/2}\,\text{Å}). \tag{4}$$

Here, double primes ($''$) are used for the initial electronic state of the Al_3^- anion and single primes ($'$) for the final state of neutral Al_3; superscript T represents a matrix transpose. $\mathbf{R}$ is the 9-vector giving the differences (Å) between the equilibrium atomic positions in the Al_3^- and Al_3 states, each with respect to its own center of mass. The normal mode vector matrix $\mathbf{N}$ contains in each of its three columns the nine Cartesian atomic displacements associated with one of the normal modes. These displacements in GAUSSIAN are normalized so that the sum of the squares of the nine values for a given normal mode is 1,[59] and the resulting $\mathbf{J}''$ matrix is orthogonal.

In C_{2v} symmetry, with the three normal modes listed in the order ν_1 (A_1, symmetric stretch), ν_2 (A_1, bend), and ν_3 (B_2, asymmetric stretch), Eq. (2) then gives

$$\mathbf{Q}'' = \mathbf{J}''\mathbf{Q}' + \mathbf{K}'',$$

$$\begin{bmatrix} Q_1'' \\ Q_2'' \\ Q_3'' \end{bmatrix} = \begin{bmatrix} \cos\phi & -\sin\phi & 0 \\ \sin\phi & \cos\phi & 0 \\ 0 & 0 & 1 \end{bmatrix}\begin{bmatrix} Q_1' \\ Q_2' \\ Q_3' \end{bmatrix} + \begin{bmatrix} \Delta Q_1'' \\ \Delta Q_2'' \\ \Delta Q_3'' \end{bmatrix}. \tag{5}$$

Here, the 2×2 A_1 block of the block-diagonal $\mathbf{J}''$ matrix is expressed as a rotation matrix giving the projections of the two A_1 normal coordinates of the anion on those of the neutral molecule. The off-diagonal elements, $J_{12} = -J_{21}$, indicate the degree of mixing between the two A_1 modes. For an $Al_3 \leftarrow Al_3^-$ photodetachment transition in which one or both states has C_{2v} symmetry, the off-diagonal $\mathbf{J}''$ matrix elements involving the B_2 asymmetric stretch, as well as the corresponding element of the $\mathbf{K}''$ displacement vector, ΔQ_3, are zero by symmetry. For a transition between D_{3h} Al_3 and Al_3^- states, the off-diagonal elements involving the symmetric stretch (the only totally symmetric mode), as well as the displacements along the degenerate bending and asymmetric stretching coordinates, ΔQ_2 and ΔQ_3, are also zero. In this case, the symmetric stretching displacement, ΔQ_1 (amu$^{1/2}$ Å), is a simple function of Δr (Å), the equilibrium bond length changes between the two states ($r_{\text{anion}} - r_{\text{neutral}}$),

$$\Delta Q_1 = (m_{Al})^{1/2}\Delta r. \tag{6}$$

For comparison with the Franck–Condon fits to the observed spectra as reported in Paper I, which employed the Hutchisson recursion method,[60] this method is also used here to generate simulated Franck–Condon spectra based on the GAUSSIAN PBE0 results. In this case, the different vibrational modes are treated independently, and Franck–Condon factors for combination bands (including transitions from excited anion vibrational levels) are obtained by multiplying those for the individual modes.[52–54] Franck–Condon factors obtained with the Hutchisson method are the same as those predicted by the method of Sharp and Rosenstock[58] with $\mathbf{J}'' = \mathbf{E}$, the identity matrix. This equality expresses the "parallel mode" approximation that the normal mode descriptions are the same in the two electronic states.

When simulating Franck–Condon spectra in the parallel mode approximation, Ervin, Lineberger, and co-workers[53,54] found that it is more accurate to use the normal mode vectors calculated for the upper state (Al_3) rather than those for the lower state (Al_3^-) as in Eqs. (2)–(5). For the present case of a homonuclear triatomic, the equations used by FCFGAUS to obtain displacements ($\mathbf{K}'$) for use in the parallel mode approximation are equivalent to the following:

$$\mathbf{Q}' = \mathbf{J}'\mathbf{Q}'' + \mathbf{K}', \tag{7}$$

where

$$\mathbf{J}' = (\mathbf{J}'')^{-1} = (\mathbf{J}'')^T \tag{8}$$

and

$$\mathbf{K}' = -(\mathbf{J}'')^T(\mathbf{K}''), \tag{9a}$$

$$\mathbf{K}' = -\sqrt{m_{\mathrm{Al}}}(\mathbf{N}')^T\mathbf{R}. \tag{9b}$$

Equation (9b) illustrates that the $\mathbf{K}'$ normal mode displacement depends on the normal mode vectors (Cartesian atomic displacements) of the final (neutral) state ($\mathbf{N}'$) rather than on those of the initial (anion) state ($\mathbf{N}''$), as does $\mathbf{K}''$ [Eq. (4)]. Equation (9a)[54] is equivalent to Eq. (9b) since $(\mathbf{N}'')^T(\mathbf{N}'') = \mathbf{E}$ due to the scaling (noted above) of the GAUSSIAN Cartesian atomic displacements. The equilibrium atomic position difference vector, $\mathbf{R}$, in Eqs. (4) and (9b) is defined by $\mathbf{R} = \mathbf{R}'' - \mathbf{R}'$ (anion minus neutral). Thus, a longer bond in the anion than in the neutral molecule corresponds to a positive value of $\mathbf{R}$ and thus to an element (ΔQ) of the normal mode displacement vector that is negative for $\mathbf{K}'$ and positive for $\mathbf{K}''$. The former ($\mathbf{K}'$) sign convention for normal mode displacements agrees with that used in Paper I.

For a transition between D_{3h} states, Eqs. (9) again give Eq. (6) for the symmetric stretching displacement except for the sign change ($\Delta r = r_{\mathrm{neutral}} - r_{\mathrm{anion}}$). For a transition between two C_{2v} states or between a C_{2v} and a D_{3h} state, however, not only the signs but also the magnitudes of $\mathbf{K}'$ and $\mathbf{K}''$ can differ. Below, we use the term "parallel mode method" to refer to the calculation of Franck–Condon factors in the harmonic, independent mode approximations, using $\mathbf{K}'$ displacements and the Hutchisson algorithms.[60]

Section SIII of the Supporting Information[61] provides a more detailed description of these Franck–Condon spectral simulation methods, and it includes numerical examples of their applications to two of the photodetachment transitions (Y and A) discussed below. In addition, through analyses of these representative $\mathrm{Al}_3 \leftarrow \mathrm{Al}_3^-$ photodetachment transitions between essentially D_{3h} states and between C_{2v} and D_{3h} states, it is shown that the Franck–Condon simulation methods[52,53] used in the present paper to predict vibronic band relative intensities and normal mode displacements ($\mathbf{K}'$) from the equilibrium geometries and vibrational properties predicted by the PBE0 calculations are consistent with those used in Paper I to deduce normal mode displacements and equilibrium bond length changes from fits to the relative vibronic band intensities observed in the photoelectron spectrum. The latter approach, which employs the Wilson GF normal mode analysis method[62] with Hutchisson Franck–Condon factors[60] as implemented by PESCAL,[52,53] is detailed in the Supporting Information for Paper I.

III. COMPUTATIONAL RESULTS

III.A. Al_3^- and Al_3 electronic states

Table I summarizes computational results for the low-lying states of Al_3^- and Al_3 with D_{3h} (equilateral triangular) or C_{2v} (isosceles triangular) equilibrium structures. States in boldface type are assigned below to transitions observed in the 488 nm anion photoelectron spectrum. For D_{3h} states, the corresponding C_{2v} symmetry is given in parentheses in Table I to facilitate comparisons with previous papers in which these labels were used. States with the same term symbol as a lower-energy state are numbered (2) or (3) in order of

increasing energy among those listed. For all of the states listed, the primarily $3s$-derived molecular orbitals (MOs) have closed-shell occupations labeled $(1a_1')^2(1e')^4$ in D_{3h} or $(1a_1)^2(2a_1)^2(1b_2)^2$ in C_{2v} symmetry. Column 2 shows the electron configurations of the MOs arising primarily from the $3p$ atomic orbitals (AOs). These are the "π-bonding" out-of-plane $1a_2''$ orbital ($1b_1$ in C_{2v}) and the in-plane "σ-bonding" $2a_1'$ orbital ($3a_1$ in C_{2v}), which are both nondegenerate in D_{3h}. At higher energies are the doubly degenerate in-plane $2e'$ ($4a_1, 2b_2$) and out-of-plane $1e''$ ($2b_1, 1a_2$) orbitals. MO pictures obtained in the present study (not shown) are similar to those previously reported for the $1a_1'$ through $2e'$ orbitals of Al_3^-.[2]

Jahn–Teller distorted pairs with single occupation of doubly degenerate e' or e'' D_{3h} orbitals are indicated in Table I by braces. As is well-known for similar systems,[7,63–65] distortion of a D_{3h} Jahn–Teller degenerate state leads to a pair of C_{2v} structures on the lower adiabatic (i.e., Born–Oppenheimer) potential energy surface. One of these is an equilibrium structure and the other is a saddle point (having one imaginary vibrational frequency) for pseudorotation into the local minimum structure. The saddle point structures are indicated by square brackets in column 1 of Table I and in the text. In addition, we will refer to the equilibrium structure (e.g., the $^3B_2$ state of Al_3^-) as a "state" or "structure" and to the saddle point (e.g., [$^3A_1$]) as a "structure."

In Table I, excitation energies (T_e) calculated using the CC (column 3) or the PBE0 (column 4) method have been converted to T_0 values (i.e., relative energies including the zero point vibrational energy) in the harmonic approximation. For Al_3, the energies relative to the Al_3 and Al_3^- ground states are both listed. Note that the PBE0 T_e energies were calculated by performing separate geometry optimizations for each structure and subtracting the resulting SCF energies; this is sometimes called the "ΔSCF" method. Column 5 of Table I gives the PBE0 geometries in terms of the two identical bond lengths of a C_{2v} structure (three in D_{3h}) and the included (apex) bond angle. Parentheses enclose the 60° bond angles of states constrained to D_{3h} symmetry in the calculations. The last column gives the PBE0 harmonic vibrational frequencies for the symmetric stretch (ν_1), bend (ν_2), and asymmetric stretch (ν_3). In D_{3h} states, ν_2 and ν_3 are degenerate (E') and ν_1 is the only totally symmetric mode ($^1A_1'$). In C_{2v} states, ν_1 and ν_2 are totally symmetric (A_1) and ν_3 has B_2 symmetry. Modes (ν_3) calculated to have imaginary frequencies are indicated by "i."

For the Al_3^- anion, the entries in Table I include all equilibrium structures and saddle points with C_{2v} or D_{3h} symmetry that were found to have energies within 0.7 eV of the ground state. Anion states, which survive the journey down the >50 cm long, 0.4–0.7 Torr flow tube anion source and are subsequently observed in the 488 nm photoelectron spectrum[35] are expected to be stable (i.e., to have at least one structure with three real vibrational frequencies) and to have relatively low calculated energies. The PBE0 calculations yielded no linear ($D_{\infty v}$ or $C_{\infty v}$) Al_3^- states meeting both criteria. The ground state of Al_3^- was found to be the D_{3h} $^1A_1'(^1A_1)$ state with a $(1a_1')^2(1e')^4(1a_2'')^2(2a_1')^2$ valence electron configuration having double occupation of all occu-

TABLE I. Summary of the computational results for D_{3h} and C_{2v} states of Al_3^- and Al_3.

State[a]	$C_{2v}\ 1b_1$ / $D_{3h}\ 1a_2''$	$3a_1$ / $2a_1'$	$4a_1\ 2b_2$ / $2e'$	$2b_1\ 1a_2$ / $1e''$	CC	CC (vs $\tilde{X}\,^1A_1'$)	PBE0	r_e (Å)	α (deg)	ν_1	ν_2	ν_3
Al_3^-												
$\tilde{X}\,^1A_1'(^1A_1)$	2	2	0 0	0 0	0.000		0.000	2.508	60.0	373	246	246
$^3B_2$	2	1	0 1	0 0	0.395		0.115	2.504	64.9	360	211	259
$[^3A_1]$	2	1	1 0	0 0	0.402		0.117	2.599	57.1	369	303	217i
$^3A_2$	1	2	0 1	0 0	0.595		0.255	2.606	65.8	313	165	212
$[^3B_1]$	1	2	1 0	0 0	0.603		0.345	2.744	54.5	342	231	88i
$^5A_2''(^5A_2)$	1	1	1 1	0 0	0.707		0.308	2.698	60.0	299	237	237
Al_3					*vs $\tilde{X}\,^1A_1'$*							
$\tilde{X}\,^2A_1'(^2A_1)$	2	1	0 0	0 0	0.000		0.000	2.507	60.0	366	244	244
					1.919 (EA)		**1.679**					
$^2A_2''(^2B_1)$	1	2	0 0	0 0	0.215	2.134	0.278	2.603	60.0	320	177	177
$^4A_2$	1	1	0 1	0 0	0.291	2.210	0.108	2.576	68.8	320	157	286
$[^4B_1]$	1	1	1 0	0 0	0.321	2.240	0.136	2.720	56.1	261	335	259i
$^2B_2$	2	0	0 1	0 0	0.735	2.654	0.726	2.509	65.1	357	220	382
$(2)^2B_2$	0	2	0 1	0 0	0.957	2.876	0.824	2.781	69.1	246	102	152
$[(2)^2A_1]$	0	2	1 0	0 0	0.959	2.878	0.946	3.073	50.2	177	302	107i
$^4A_1'(^4B_2)$	0	1	1 1	0 0	1.079	2.998	0.880	2.897	60.0	237	195	195
$^4A_2''((2)^4A_2)$	1	0	1 1	0 0	f		1.026	2.737	(60.0)	282	256	256
$(2)\,^4B_2$	1	1	0 0	0 1	1.842	3.761	1.606	2.595	76.1	277	100	167
$[^4A_1]$	1	1	0 0	1 0	1.874	3.793	1.651	2.878	51.6	170	295	142i
$^2A_2$	0	2	0 0	0 1	f		2.507	2.725	87.5	214	71	145
$(2)^2A_2$	2	0	0 0	0 1	2.426	4.345	2.471	2.540	69.2	308	162	191
$[(2)\,^2B_1]$	2	0	0 0	1 0	2.442	4.361	2.504	2.730	53.3	223	357	281i
$(2)\,^4A_2''((3)\,^4A_2)$	1	0	0 0	1 1	3.833	5.752	3.701	3.070	(60.0)	115	127	127

[a]States in bold are assigned to transitions in the 488 nm photoelectron spectrum. Symmetry labels for D_{3h} states are accompanied by corresponding C_{2v} labels in parentheses. Label (n) preceding a term symbol refers to the nth state of that type among those listed. Braces indicate Jahn–Teller distorted pairs of A_1 and B_2 (E' in D_{3h}) or B_1 and A_2 (E'') structures and square brackets (e.g., $[^3A_1]$) indicate the saddle point structure in each pair, having an imaginary calculated ν_3 frequency.

[b]All states listed have a filled $(1a_1)^2\ (2a_1)^2\ (1b_2)^2$ electronic configuration [$(1a_1')^2\ (1e')^4$ in D_{3h}] for the lower-energy MOs derived primarily from the 3s AOs. For example, the valence electron configuration for the $\tilde{X}\,^1A_1'(^1A_1)$ Al_3^- ground state is $(1a_1')^2(1e')^4(1a_2'')^2(2a_1')^2$ using D_{3h} labels or $(1a_1)^2(2a_1)^2(1b_2)^2(1b_1)^2(3a_1)^2$ using C_{2v} labels.

[c]Relative energies of the zero point vibrational levels of the states (that is, T_0 values), where the zero point energies are calculated in the harmonic approximation from the PBE0/MG3 frequencies. Note that $T_0=T_e+\Delta$ZPE, where ΔZPE is the zero point energy difference of the two states (upper minus lower). CCSD(T)/CBS//PBE0/MG3 T_e values are calculated at the aug-cc-pVxZ, $x=\{D,T,Q\}$ level at the PBE0/MG3 optimized geometries and are extrapolated to the complete basis set limit.

[d]Geometries (PBE0/MG3) give the length of the identical bonds and the included angle. States marked (60°) were calculated assuming D_{3h} symmetry.

[e]Frequencies (PBE0/MG3) are labeled ν_1 [symmetric stretch of two (C_{2v}) or three (D_{3h}) equivalent bonds], ν_2 ("bend," mainly the unique bond stretch in C_{2v} states), and ν_3 (asymmetric stretch). For the four C_{2v} Al_3 structures with bond angles of <60° and an imaginary ν_3 frequency, the bend is calculated to be the higher frequency, and the symmetric stretch the lower frequency, of the two A_1 modes.

[f]See Sec. III.A for discussion of states for which CC energies are not listed.

pied MOs [$(1a_1)^2(2a_1)^2(1b_2)^2(1b_1)^2(3a_1)^2$ using C_{2v} labels], in agreement with the results of previous calculations.[1–5,15,19,21] This state and the $^5A_2''(^5A_2)$ excited state, in which the doubly degenerate e' orbitals are each singly occupied, are not Jahn–Teller distorted; as expected, calculations assuming a C_{2v} geometry optimized to essentially equilateral structures with 60.00° bond angles. The remaining structures of Al_3^- in Table I include two C_{2v} Jahn–Teller distorted pairs in which the $2e'(4a_1,2b_2)$ orbital is singly occupied. In the lower-energy $^3B_2$ or $^3A_2$ states, the $2b_2$ occupied MO is antibonding with respect to the unique base bond, giving a C_{2v} geometry with an apex (unique) bond angle of >60°. The higher-energy $[^3A_1]$ and $[^3B_1]$ saddle points have apex bond angles of <60°, as expected in view of the bonding character of the $4a_1$ orbital with respect to the base (unique) bond.

TABLE II. Comparison of computational to experimental results. [Experimental results (in italics) are from Paper 1 (Ref. 35, Table II) except as noted.]

State	Energy (eV)[a]		CC energy (eV)[b] vs anion state		Equilibrium geometry[c]		Frequencies (cm⁻¹)		Force constants[d] (mdyn/Å)	
	CC	PBE0	$\widetilde{X}\,^1A_1'$	$^3B_2$	r_e (Å)	α (deg)	ν_1	ν_2		
Al_3^-										
$\widetilde{X}\,^1A_1'$ ($^1A_1$)	0.000	0.000			2.508	60.0	373	246	$f(r), f(rr)$	0.673, 0.032
	0.000				*2.51±0.02*		*365±15*	*257±15*	*0.70±0.06, 0.00±0.03*	
						60.0±0.4				
$^3B_2$	0.395	0.115			2.504	64.9	360	211	$f(r), f(r_b)$	0.739, 0.425
	0.409±0.004				*2.51±0.01*		*330±20*	*200±10*	$f(rr), f(rr_b)$	0.059, −0.011
						65.0±0.7			*0.65±0.04, 0.40±0.03*	
Al_3										
$\widetilde{X}\,^2A_1'$ ($^2A_1$)	0.000	0.000	1.919 (X,EA)	1.524 (A)	2.507	60.0	366	244	$f(r), f(rr)$	0.659, 0.026
	0.000		*1.916±0.004*	*1.507±0.003*	*(Assumed)[c]*		*357±10* [e]	*240±10*	*0.63±0.04, 0.02±0.02*	
								245±2[f]		
$^2A_2''$ ($^2B_1$)	0.215	0.278	2.134 (Y)	1.739 (B)	2.603	60.0	320	177	$f(r), f(rr)$	0.403, 0.069
	0.192±0.004		*2.108±0.005*	*1.699±0.004*	*2.61±0.03*		*315±15*	*197±10*	*0.45±0.03, 0.04±0.02*	
						60.0±2.0	*319±2*[f]			
$^4A_2$	0.291	0.108		1.815 (C)	2.576	68.8	320	157	$f(r), f(r_b)$	0.736, 0.230
	0.300±0.004			*1.807±0.004*	*2.57±0.02*		*315±15*	*140±10*	$f(rr), f(rr_b)$	−0.058, −0.019
						69.0±1.5			*0.64±0.03, 0.19±0.02*	
$^2B_2$	0.735	0.726		2.259 (D)	2.509	65.1	357	220	$f(r), f(r_b)$	1.157, 0.443
	0.706±0.005			*2.213±0.006*	*2.51±0.04*				$f(rr), f(rr_b)$	−0.312, −0.060
						65.0±2.5				

[a]Energies (T_0) with respect to the ground state zero point level of the same species (see Table I notes).

[b]CCSD(T)/CBS//PBE0/MG3 energies with respect to those of the Al_3^- $\widetilde{X}\,^1A_1'$ ($^1A_1$) (for transitions X and Y) and $^3B_2$ (for transitions A-D) states, including zero point contributions (see Table I notes). EA=electron affinity.

[c]In C_{2v} states, α is the bond angle between the two identical bonds of length r_e. Experimental results are obtained from Franck–Condon fits to the photoelectron spectra by assuming the calculated Al_3 $\widetilde{X}\,^2A_1'$ geometry.

[d]PBE0 force constants in internal coordinates multiplied by $m/\sqrt{3}$ (where $m=26.98$), from D_{3h} calculations for $\widetilde{X}\,^1A_1'$, $\widetilde{X}\,^2A_1'$, and $^2A_2''$ states and from C_{2v} calculations for other states. Primary stretching force constants are $f(r)$ and $f(r_b)$ (for the two identical bonds and the unique base bond, respectively, in C_{2v} states) and interaction constants are $f(rr)$ and $f(rr_b)$. Experimental values for C_{2v} states ($^3B_2$ Al_3^- and $^4A_2$ Al_3) list $f(r), f(r_b)$, and assume zero interaction constants.

[e]Al_3 $\widetilde{X}\,^2A_1'$ ($^2A_1$) ground state fundamental frequencies suggested by the reinterpretation of the R2PI spectra (Refs. 38 and 40) in Sec. IV.A are 351 cm⁻¹ (ν_1) and 235 cm⁻¹ (ν_2 and ν_3). The latter value assumes an harmonic bending potential in the upper R2PI state, so that the $\nu'=1$ fundamental frequency is half the observed $\nu'=2$ value.

[f]Frequencies in a neon matrix (Ref. 41).

For neutral Al_3, Table I lists three states for which C_{2v} calculations optimized to essentially D_{3h} geometries. These are the $\widetilde{X}\,^2A_1'(^2A_1)$ ground state and the $^2A_2''(^2B_1)$ first excited state, in which both occupied valence orbitals are non-degenerate, and the $^4A_1'(^4B_2)$ state, in which both $2e'$ orbitals are singly occupied. Two other quartet states, $(1a_2'')^1(2e')^2\,^4A_2''((2)^4A_2)$ and $(1a_2'')^1(2e'')^2\,(2)^4A_2''((3)^4A_2)$, were constrained to D_{3h} symmetry to retain the indicated MO occupations in the PBE0 calculations and to prevent relaxation to lower-energy states with the same C_{2v} occupied orbital symmetries. The C_{2v} states listed include four Jahn–Teller distorted states (whose degenerate $2e'$ or $1e''$ D_{3h} orbital would be singly occupied), for each of which results are again tabulated for both the equilibrium and the saddle point structures. In each of these pairs, the former structure has an occupied $2b_2(2e')$ or $1a_2(1e'')$ orbital, giving an apex bond angle of $>60°$. The latter, saddle point structure has an occupied $4a_1(2e')$ or $2b_1(1e'')$ orbital and an apex bond angle of $<60°$. This reduced bond angle results in a frequency reversal of the two A_1 vibrational modes in these four Al_3 saddle point structures, with the symmetric stretch of the two identical, longer side bonds having a lower frequency than the "bending" mode, which involves mainly the stretch of the shorter, base bond.

Table I includes CC energies for 17 excited-state structures (5 for Al_3^- and 12 for Al_3). The excitation energies of 16 of these structures at the CCSD(T)/QZ level, relative to the ground state of the same species calculated by the same method, were lower than those obtained at the CBS level by 0.01–0.04 eV (average of 0.02 eV). [For the high-energy $(2)^4A_2''$ state, the QZ excitation energy was 0.13 eV lower.] With the TZ basis set, the CCSD(T) excitation energies of these 16 structures were lower than those obtained at the CBS level by 0.02–0.11 eV (average of 0.06 eV). CC energies are not listed for the $^2A_2$ state for the reasons discussed in the following paragraph, or for the $^4A_2''((2)^4A_2)$ state, which relaxed in MOLPRO to the lower-energy $^4A_2$ state.

Table S-I in the Supporting Information[61] lists CCSD(T)/QZ (quadruple ζ) total energies, T_1 diagnostics, and spin contamination values ($\langle S^2 - S_z^2 - S_z\rangle$). The $\langle S^2\rangle$ values obtained in the PBE0/MG3 calculations are also included. T_1 diagnostic values were ≤ 0.037 for 18 of the 19 structures of

TABLE III. Comparison of calculated to experimental normal mode displacements.

| Transition | e^- Detachment | | | $\mathbf{J''}$a | | $\mathbf{K''}$ b,c | $\mathbf{K'}$ b,d | Experimental $\mathbf{\Delta Q}$ b,e |
	C_{2v} / D_{3h}: $1b_1$ / $1a_2''$	$3a_1$ / $2a_1'$	$2b_2$ / $2e'$	$J_{1,1}$	$J_{1,2}$			
X $^2A_1' \leftarrow {}^1A_1'$	0	1	0	1.000	0.000	0.005	−0.005	$\pm 0.045\ \Delta Q_1$
						0.000	0.000	$\pm 0.050\ \Delta Q_2$
Y $^2A_2'' \leftarrow {}^1A_1'$	1	0	0	1.000	0.001	−0.494	0.494	0.54
						0.001	0.000	$<|0.25|$
A $^2A_1' \leftarrow {}^3B_2$	0	0	1	0.969	−0.247	0.128	−0.298	−0.33
						0.700	−0.646	−0.64
B $^2A_2'' \leftarrow {}^3B_2$		$(2e^-)$		0.969	−0.248	−0.355	0.201	0.20
						0.576	−0.646	−0.60
C $^4A_2 \leftarrow {}^3B_2$	1	0	0	0.997	0.074	−0.460	0.409	0.46
						−0.673	0.705	0.63
D $^2B_2 \leftarrow {}^3B_2$	0	1	0	0.996	0.092	−0.031	0.028	$<|0.15|$
						−0.030	0.033	$<|0.15|$

aCalculated $J_{1,1}$ and $J_{1,2}$ elements of the $\mathbf{J''}$ (Duschinsky rotation) matrix describing the normal modes of the initial state (Al₃⁻, Q'') in terms of those of the final state (Al₃, Q') for the two A_1 C_{2v} modes. $J_{2,1} = -J_{1,2}$ and $J_{2,2} = J_{1,1}$, where row 1 of $\mathbf{J''}$ describes the symmetric stretch (Q_1'') and row 2 the bend (Q_2'').
bDisplacements $\mathbf{K''}$, $\mathbf{K'}$, and $\mathbf{\Delta Q}$ in amu$^{1/2}$ Å for the symmetric stretch (top row) and bend (bottom row). Asymmetric stretching displacements are zero. The sign convention used here is that a shorter bond in the initial (Al₃⁻) than in the final (Al₃) state corresponds to a normal mode displacement that is negative for $\mathbf{K''}$ and positive for $\mathbf{K'}$ and $\mathbf{\Delta Q}$.
cCalculated $\mathbf{K''}$ normal mode displacement vector: $\mathbf{Q''} = \mathbf{J''Q'} + \mathbf{K''}$ [Eq. (2)].
dCalculated $\mathbf{K'}$ normal mode displacement vector: $\mathbf{Q'} = \mathbf{J'Q''} + \mathbf{K'}$ with $\mathbf{K'} = -(\mathbf{J''})^T\mathbf{K''}$ [Eqs. (7) and (9)].
eExperimentally determined magnitudes of normal mode displacements ($\pm 10\%$) ΔQ_1 for the symmetric stretch and ΔQ_2 for the bend, obtained in the parallel mode approximation, with suggested signs, from Paper I (Ref. 35, Table II).

Al₃⁻ or Al₃ for which CCSD(T)/CBS energies are listed in Table I; the exception was [$^4A_1$] Al₃ ($T_1 = 0.059$). A T_1 value of ≤0.044 has been used in unrestricted CCSD(T) calculations as a threshold for the suitability of this single-reference method.[66,67] For the $^2A_2$ state of Al₃, although the T_1 value (0.042) falls below this threshold, results show substantial spin contamination (0.358) and an anomalous *in*crease in energy (by 0.19 eV) upon improving the basis set from triple to quadruple ζ. Other states for which the results indicated a relatively high degree of spin contamination in the CC and/or PBE0 calculations were the $^3A_2$ state of Al₃⁻ and the $(2)^2B_2$ and $(2)^2A_2$ states of Al₃. These five states are not among those observed in the 488 nm photoelectron spectrum, according to the assignments in Sec. III.B.

CC energies for the triplet and quintet excited-state structures of the Al₃⁻ anion, relative to that of the singlet $\tilde{X}\ ^1A_1'(^1A_1)$ ground state calculated by the same method, are found to be significantly higher than those obtained by the PBE0 density functional method. Excitation energy differences between the two methods were 0.26–0.34 eV for the four triplet structures listed in Table I and 0.40 eV for the quintet state. The Al₃ electron affinity (EA) was predicted to be 0.240 eV lower using PBE0 (1.679 eV) than CC (1.919 eV). For Al₃, the PBE0 energies of the six doublet excited-state structures, which have the same spin multiplicity as the ground state, all fell within ±0.1 eV of the CC value, with an average unsigned difference of only 0.05 eV. For Al₃, excluding the $(2)^2B_2$ state for which both calculations showed relatively high spin contamination as noted above, the five doublet excited-state structures showed CC excitation energy values from 0.01 eV higher to 0.06 eV lower than the PBE0 values, with an average unsigned difference of only 0.038 eV. However, for the six quartet struc-

tures for which CC energies were obtained, the PBE0 energies, relative to the doublet ground state, were 0.13–0.24 eV (average of 0.19 eV) lower than the CC values. These results for the Al₃ quartets and for the Al₃⁻ triplets and quintets reflect the tendency of hybrid DFT with 25% HF exchange to overestimate the relative stabilities of high-spin states. This bias also results in a different energy ordering for the low-energy Al₃ states calculated by the two methods. The PBE0 results give the $^4A_2$(0.108 eV) as the lowest excited state, 0.17 eV below the $^2A_2''(^2B_1)$ state at 0.278 eV. In contrast, the latter state is identified by the CC method as the first excited state (0.215 eV), with the $^4A_2$(0.291 eV) predicted to be 0.076 eV higher in energy.

Several other Al₃ states which may also fall in this energy range are not included in Table I. For example, the $^2B_2$ and $^2A_2$ states, which are listed in the table, are Jahn–Teller distorted states whose [$^2A_1$] and [$^2B_1$] structures [with an occupied $4a_1(2e')$ or $2b_1(1e'')$ orbital, respectively] could not be characterized by SCF calculations, since they have the same occupied orbital symmetries as lower-energy states. PBE0 results for a [$^2B_2$] structure having single occupation of the primarily 3s-derived $1b_2$ orbital [$(1a_1)^2(2a_1)^2(1b_2)^1(1b_1)^2(3a_1)^2$, where the $2a_1$ and $1b_2$ orbitals correspond to the degenerate $1e'\ D_{3h}$ orbital], displayed significant spin contamination [$\langle S^2 \rangle = 1.68$ versus the 0.75 ideal $S(S+1)$ value for a doublet state]. These calculations gave an excitation energy (T_0) of 2.45 eV, an imaginary ν_3 frequency, a 2.63 Å bond length, and a 52° apex bond angle for this [$^2B_2$] structure. The Jahn–Teller paired $^2A_1$ [$(1a_1)^2(2a_1)^1(1b_2)^2(1b_1)^2(3a_1)^2$] C_{2v} state, as well as the $^2A_1'(^2A_1)$ D_{3h} state in which the $1a_1'(1a_1)$ 3s-derived orbital is singly occupied, could not be characterized by this DFT method due to the presence of lower-energy states with the

same occupied orbital symmetries. Attempts to identify excited D_{3h} states with single occupation of a higher-energy nondegenerate $3a_1'$ or $2a_2''$ orbital were also not successful using either the PBE0 SCF calculations or the time dependent PBE0 method.

III.B. Photodetachment transitions

Figures 1–3 display simulated photodetachment transitions (dashed lines) based on the calculated PBE0 geometries and vibrational properties of the Al_3^- and Al_3 states. Following Paper I,[35] the six observed photodetachment transitions are labeled X and Y (observed under both room temperature and cooled flow tube conditions) and A-D (observed only under cooled flow tube conditions). In each transition, the position and intensity of the origin band ($v'_{\text{neutral}}=0 \leftarrow v''_{\text{anion}}=0$, labeled 0_0^0) in the simulated spectrum were chosen to match those in the observed spectrum (solid line, from Paper I).[35] The positions of the other vibronic bands in the same simulated photodetachment transition are shown relative to that of its origin, and their intensities are scaled by the same factor. As in Paper I, no additional intensity scaling based on the electron velocity[55] is applied. Vibronic bands are labeled $v_{v''}^{v'}$, where $v=1$ for the symmetric stretch, $v=2$ for the bend, and $v=3$ for the asymmetric stretch, and v'' and v' are the vibrational quantum numbers of mode v in the initial (Al_3^-) and final (Al_3) states, respectively. (For example, 2_0^1 represents a transition in the bend from $v_2''=0$ in Al_3^- to $v_2'=1$ in Al_3.) Relative intensities of transitions from excited vibrational levels of the anion are calculated assuming the same anion vibrational temperatures as were obtained in Paper I from Franck–Condon fits to the corresponding spectra. The individual vibronic transitions, represented by sticks, were also convoluted with Lorentzian line shapes with the same widths (noted in the figure captions) as were used in Paper I.

Table II compares the calculated and experimental (in italics) results for the observed transitions, assigned as discussed below, for the energies, geometries, vibrational frequencies, and force constants. The GAUSSIAN PBE0 force constants were multiplied by $m/\sqrt{3}$, where m is the Al atomic mass, to remove the reduced mass weighting for comparison with the force constants obtained in Paper I using the Wilson GF matrix method.[62] This method was also used in Paper I to obtain the experimental results for the equilibrium geometries listed in Table II, which assumed the PBE0 calculated equilibrium geometry for the $\widetilde{X}\,^2A_1'(^2A_1)$ Al_3 ground state.

Table III summarizes, for each of the six observed photodetachment transitions, the calculated $\mathbf{J}''$, $\mathbf{K}''$, and $\mathbf{K}'$ matrix elements for the two A_1 C_{2v} modes [Eq. (3), (4), and (9)]. For the calculated $\mathbf{K}''$ and $\mathbf{K}'$ elements and the experimental (ΔQ) normal mode displacement values, which have units of $amu^{1/2}$ Å, the first row gives the normal mode displacement for v_1, the symmetric stretch, and the second row for v_2, the bend.

Summaries of the GAUSSIAN output files, which include the results used to generate the Franck–Condon simulations in Figs. 1–3, are provided in the Supporting Information.[61]

III.B.1. Transition X

Figure 1 displays two calculated photoelectron transitions, labeled X and Y, from the D_{3h} $\widetilde{X}\,^1A_1'(^1A_1)$ ground state of Al_3^-. Transition X accesses the $\widetilde{X}\,^2A_1'(^2A_1)$ $[(1a_2'')^2(2a_1')^1]$ D_{3h} ground state of Al_3 $[(1b_1)^2(3a_1)^1$ using C_{2v} labels] by detachment of an electron from the filled $2a_1'(3a_1)$ anion highest occupied MO (HOMO). As indicated in Table I, the energy difference between the zero point vibrational levels of the two states, i.e., the adiabatic EA of Al_3, is calculated to be 1.919 eV at the CC level. This result can be further improved through the inclusion of additional terms for core-valence interactions (ΔE_{CV}) and relativistic effects (ΔE_{SR}).[4] These contributions were found to lower the ground state energy of Al_3 relative to that of Al_3^- (i.e., to decrease the EA) by 0.021 eV for ΔE_{CV} and by 0.006 eV for ΔE_{SR}, giving a total correction of 0.027 eV. The resulting calculated EA of Al_3 is 1.892 eV, as previously reported (1.89 eV).[4] These improved CC results differ by only 0.024 eV (1%) from the measured value of 1.916 ± 0.004 eV. In contrast, the PBE0 EA of 1.679 eV is 0.24 eV (12%) lower than experiment.

As indicated in Table II, the PBE0 calculated frequencies for the Al_3 (366, 244 cm^{-1}) and Al_3^- (373, 246 cm^{-1}) ground states also fall within the experimental uncertainties of the v_1 and v_2 frequencies measured from the photoelectron spectrum, and the 244 cm^{-1} calculated v_2 value also agrees with
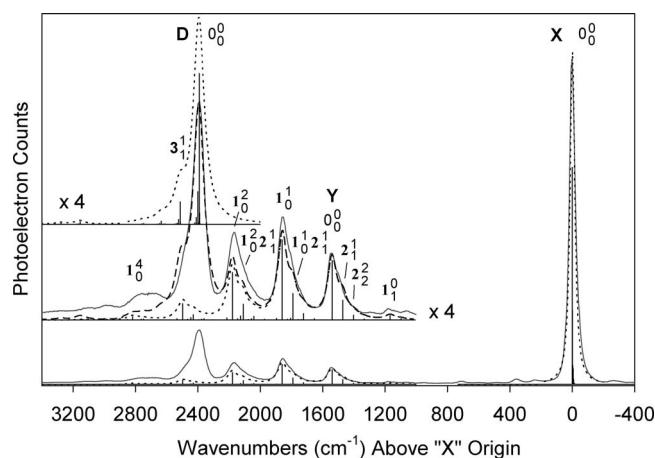

FIG. 1. Comparison of the observed 488 nm (2.54 eV) $Al_3 \leftarrow Al_3^-$ photoelectron spectrum of anions prepared in the short liquid nitrogen cooled flow tube (solid line) with predicted spectra from PBE0 calculations (dashed lines and sticks) for $\widetilde{X}\,^2A_1'(^2A_1) \leftarrow \widetilde{X}\,^1A_1'(^1A_1)$ (transition X), $^2A_2''(^2B_1) \leftarrow \widetilde{X}\,^1A_1'(^1A_1)$ (transition Y), and $^2B_2 \leftarrow {}^3B_2$ (transition D). Franck–Condon factors are calculated by the SRC method. For each transition, the origin band (0_0^0) position and intensity are chosen to match the observed spectrum. Assignments are given as $v_{v''}^{v'}$, where $v=1$ for the symmetric stretch, $v=2$ for the bend, and $v=3$ for the asymmetric stretch, and v'' and v' are the vibrational quantum numbers of mode v in the initial (Al_3^-) and final (Al_3) states, respectively. For transition Y between states with D_{3h} equilibrium structures, the label 2_1^1 also represents 3_1^1, and 2_2^2 also represents 3_2^2 and $2_1^13_1^2$; stick heights are summed for degenerate or nearly degenerate transitions. For overlapping transitions Y and D, which are expanded (four times) in the middle and upper spectra, the short dashed line shows the individual transitions (for Y in the middle and for D in the upper spectra) and the long dashed line (in the middle spectrum) shows their sum. Anion vibrational temperatures of 200 K are assumed and sticks are convoluted with Lorentzian line shapes with widths of 5, 10, and 12 meV for transitions X, Y, and D, respectively, as in Paper I.
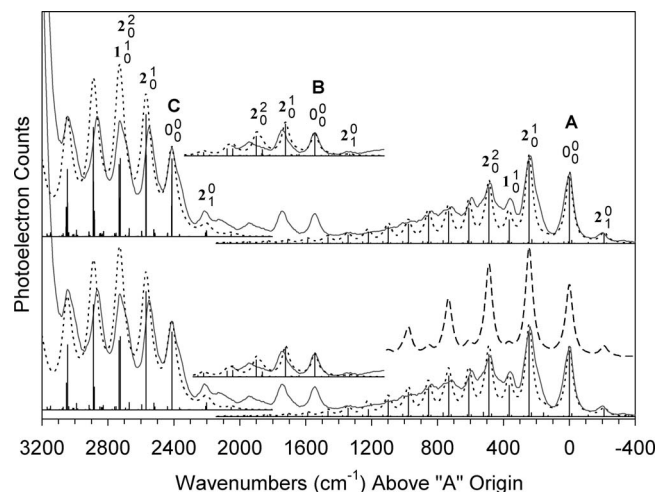
FIG. 2. Comparison of the observed spectra for Al_3^- anions prepared in the long liquid nitrogen cooled flow tube (solid line) with predicted spectra from PBE0 calculations (dashed lines and sticks) for transitions from the excited $^3B_2$ state of Al_3^- to the $\widetilde{X}\,^2A_1'(^2A_1)$, $^2A_2''(^2B_1)$, and $^4A_2$ states of Al_3 for transitions A, B, and C, respectively. Notation as in Fig. 1; e.g., 2_0^1 represents the transition from $v''=0$ of Al_3^- to $v'=1$ of Al_3 in normal mode 2, the bend. Origin band (0_0^0) positions and intensities are fit to the observed values. As in Paper I, the assumed vibrational temperatures are 160 K for the symmetric stretch (ν_1) and 120 K for the bend (ν_2) and asymmetric stretch (ν_3), and transitions are convoluted with Lorentzian line shapes with widths of 7.5 meV for A and B and 10 meV for C. Top panel: Harmonic Franck–Condon factors calculated by the SRC method using $\mathbf{K}''$ displacements. Bottom panel: Harmonic Franck–Condon factors calculated in the parallel mode approximation using $\mathbf{K}'$ displacements for transitions A, B, and C (short dashed lines and sticks) or $\mathbf{K}''$ displacements for transition A (long dashed lines).

the 245 ± 2 cm^{-1} frequency measured for Al_3 in a neon matrix.[41] As is also noted in the table, $f(r)$ and $f(rr)$, the principal and interaction force constants predicted in the PBE0 D_{3h} calculations, also agree with the values obtained from the measured frequencies in Paper I.

In contrast to the weak vibrational activity in both the symmetric stretch and the bend observed in transition X (Paper I, Fig. 3), the calculated spectrum does not exhibit activ-
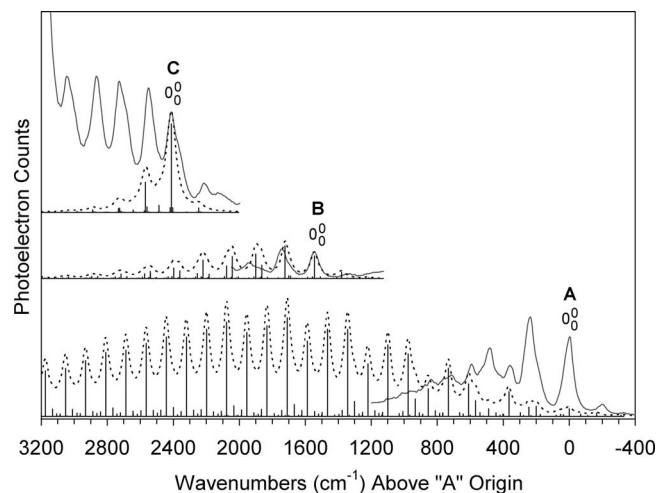

FIG. 3. As in Fig. 2, for transitions from the excited $^3A_2$ state of Al_3^-. Franck–Condon factors are calculated using the Duschinsky SRC method with $\mathbf{K}''$ displacements. For transition A, the intensity of the origin transition is 10% that in Fig. 2.

ity in the bend ($\Delta Q_2=-0.0001$ amu$^{1/2}$ Å) since both states have essentially D_{3h} equilibrium structures. As indicated in Table III, the calculated symmetric stretching displacement ($\Delta Q_1=-0.005$ amu$^{1/2}$ Å) is also lower than the measured value (±0.045 amu$^{1/2}$ Å). However, these differences are small, and the calculated bond length difference of 0.001 Å between the Al_3^- (2.508 Å) and Al_3 (2.507 Å) ground states falls within the 0.00 ± 0.02 Å difference deduced from the data in Paper I. As has previously been reported, equal bond lengths of 2.544 Å are obtained for the two states at the CCSD(T)/aug-cc-pVTZ level,[4] and the present CCSD(T) calculations also find equal bond lengths (r_e) of 2.527 Å at the QZ and 2.517 Å at the CBS levels. As noted in Paper I (Fig. 3), the intensities of the 1_0^2 and 1_0^3 stretching overtones are anomalous even in the fitted spectrum, and it is possible that the 1_0^1 and 2_0^1 fundamental band intensities (from which the experimental normal mode displacements were obtained) may also diverge from the expected Franck–Condon behavior.

III.B.2. Transition Y

Transition Y is assigned to the excited $^2A_2''(^2B_1)$ state, which is the only other Al_3 state calculated to be accessible from the Al_3^- ground state in a one-electron process within the energy window of the 488 nm (2.540 eV) photoelectron spectrum. This first excited Al_3 state is accessed by detachment of an electron from the out-of-plane, π-bonding $1a_2''(1b_1)$ orbital. The calculated adiabatic electron detachment energy for the $^2A_2''\leftarrow\widetilde{X}\,^1A_1'(^1A_1)$ transition is 2.134 eV, close to the measured value of 2.108 ± 0.005 eV. In addition, the calculated 320 cm^{-1} symmetric stretching frequency is consistent with the 315 ± 15 cm^{-1} value measured from the photoelectron spectrum and with the 319 ± 2 cm^{-1} frequency reported for matrix-isolated Al_3.[41] The vibrational structure predicted for transition Y is also shown in Fig. 1 (short dashed spectrum). The agreement with the experimental spectrum is very good, with both spectra displaying a progression in the symmetric stretch with sequence bands in the degenerate bend (ν_2) and asymmetric stretch (ν_3) (e.g., $\Delta\nu_2=\nu_2'-\nu_2''=0$) shading each peak to the red (low-energy side). As is also the case for transition X, the Al_3^- and Al_3 states are both calculated to have D_{3h} equilibrium geometries, so $\Delta Q_2=\Delta Q_3=0$ and odd $\Delta\nu$ transitions in the two inactive, nontotally symmetric modes have zero calculated intensities. The displacement in the symmetric stretch (Table III, ΔQ_1) is about 10% lower than measured (falling just within the $\pm10\%$ experimental uncertainty), and the simulated transition intensities to the higher ν_1' levels in Fig. 1 appear too weak. As indicated by Eq. (6), a 10% difference between the measured and calculated ΔQ_1 values would correspond to a ~0.01 Å underestimate in the calculated bond elongation (0.095 Å) upon electron detachment. A similar bond elongation of 0.092 Å has been reported based on calculations performed at the CCSD(T)/aug-cc-pVTZ level.[4]

III.B.3. Transition A

Figure 2 displays simulated photodetachment transitions A-C from the first excited anion state, the $C_{2v}\,^3B_2$ state. For

A, the dashed line in the top panel shows the predicted Franck–Condon spectrum for this transition from the $^3B_2$ $((1b_1)^2(3a_1)^1(2b_2)^1)$ anion state to the $\widetilde{X}\,^2A_1'(^2A_1)$ ground state of Al_3, which involves detachment of the $2b_2$ electron. The simulated and experimental spectra (solid line) agree well, and the calculated adiabatic electron detachment energy of 1.524 eV is close to the observed value of 1.507 ± 0.003 eV. As indicated in Table II, the geometry of the $^3B_2$ anion state deduced from the data in Paper I (2.51 ± 0.01 Å, $65.0 \pm 0.7°$), which was based on assuming the calculated $\widetilde{X}\,^2A_1'$ geometry for the neutral species, is also consistent with the $^3B_2$ calculated geometry (2.504 Å, 64.9°). It is interesting to note that the calculated principal force constants for the identical side bonds of the $C_{2v}\,^3B_2$ state (0.739 mdyn/Å) are substantially higher than for the longer base bond (0.425 mdyn/Å), despite the small deviation (5°) from a 60° apex bond angle. The stretch-stretch interaction force constant between the two side bonds ($f(rr)$) is calculated to be $+8\%$ of $f(r)$, and the interaction constant between the side and base bonds ($f(rr_b)$) is calculated to be -2% of the average value of the two principal force constants.

Since transition A involves a C_{2v} anion and D_{3h} neutral molecule, the 2×2 A_1 block of the $\mathbf{J}''$ matrix has significant off-diagonal elements with $J_{12} = -J_{21} = -0.25$ and $J_{1,1} = J_{2,2} = 0.97$ (Table III). Thus, the $\mathbf{K}''$ [Eq. (4)] matrix elements (0.128 and 0.700 amu$^{1/2}$ Å) differ in magnitude from those obtained in Paper I using the parallel mode approximation ($\Delta Q_1 = -0.33$, $\Delta Q_2 = -0.64$ amu$^{1/2}$ Å), although the geometry displacements deduced from the latter values agree with those calculated, as noted above. A more direct comparison can be made with the $\mathbf{K}'$ [Eqs. (9)] calculated displacements (-0.298, -0.646), which agree to within experimental error ($\pm 10\%$) with the experimental values. The bottom panel of Fig. 2 displays the simulated Franck–Condon spectrum obtained using these $\mathbf{K}'$ values and the Hutchisson formulas[60] in the parallel mode approximation, as compared with the SRC treatment in the top panel using $\mathbf{K}''$ displacements, for the same calculated geometries and vibrational frequencies. Despite the significant off-diagonal $\mathbf{J}''$ matrix elements, the differences between the two treatments, with respect to the relative vibronic band intensities predicted, are slight. Thus, for the modest degree of mode mixing and vibrational excitation displayed in transition A, the parallel mode approximation appears adequate provided that $\mathbf{K}'$ displacements are used. That is, the normal mode displacement should be expressed in terms of the normal modes of the upper (neutral) state [Eq. (9b)], as has been emphasized by Ervin and co-workers.[53,54] On the other hand, as shown for transition A in the simulation in the middle panel of Fig. 2 (long dashed lines), the combination of the $\mathbf{K}''$ calculated displacements with the parallel mode approximation, as implemented by the Hutchisson method, yields predicted vibronic band intensities that differ significantly from those observed.

As illustrated in Fig. 3, in contrast to the excellent agreement with experiment obtained for the $\widetilde{X}\,^2A_1' \leftarrow\,^3B_2$ assignment for transition A, very poor agreement is obtained if this transition is assigned instead as $\widetilde{X}\,^2A_1' \leftarrow\,^3A_2$, arising from the second stable excited state of the anion. This simulated spec-

trum shows a long symmetric stretching progression in the 366 cm^{-1} ν_1' Al_3 ground state interval due to the large equilibrium bond length change (2.606 Å Al_3^-, 2.507 Å Al_3), combined with a weaker bending progression in the 244 cm^{-1} ν_2' interval, with overlapping combination bands ($2\nu_1' = 3\nu_2'$). In addition, the calculated photodetachment energy of 1.324 eV (1.919–0.595 eV) for this alternative assignment is substantially lower than the observed value (1.507 eV).

Several other possible assignments for the initial Al_3^- state of transition A can be considered. In a previous (UV) photoelectron spectrum, this transition (labeled X′) was assigned to (what we refer to here as) the $[^3A_1]$ excited-state structure. Although its calculated energy (0.402 eV) is quite close to that of the $^3B_2$ state (0.395 eV), the $[^3A_1]$ assignment can be rejected on the following grounds. The Al_3 vibrational intervals observed in transition A match those in transition X (Table I of Paper I), indicating that transition A also accesses the $\widetilde{X}\,^2A_1'$ Al_3 ground state. The long calculated $[^3A_1]$ bond length (2.599 Å) is close to that of the $^3A_2$ state (2.606 Å), so a $\widetilde{X}\,^2A_1' \leftarrow [^3A_1]$ transition would also be accompanied by a long progression in the symmetric stretch (as in Fig. 3), which is not observed. In addition, the anion bending frequency for transition A ($\nu_2'' = 200$ cm^{-1}) differs substantially from the calculated $[^3A_1]$ bending frequency (303 cm^{-1}). Moreover, although the $[^3A_1]$ structure had been thought to be a local minimum[36] based on the available calculations,[12] the present results find it to be a saddle point (having an imaginary ν_3 calculated frequency). The higher-energy $[^3B_1]$ structure is calculated to have an even longer bond length (2.744 Å), so a transition to the $\widetilde{X}\,^2A_1'$ Al_3 ground state would produce an even more extensive stretching progression. In addition, the calculated energy of the $[^3B_1]$ structure (0.603 eV) would give a detachment energy of only 1.316 eV, substantially lower than the observed 1.507 eV value. The quintet $^5A_2''$ state can be ruled out since a transition to the doublet Al_3 ground state would be spin forbidden. Therefore, of the five calculated low-energy excited-state structures of Al_3^- in Table I, only the $^3B_2$ provides a reasonable assignment for the initial anion state of transition A.

III.B.4. Transition B

Figure 2 also shows the observed (solid line) spectrum of transition B, whose origin band is measured to lie 1545 ± 20 cm^{-1} above that of transition A. The calculated spectrum (dashed line) is shown for a transition from the same excited Al_3^- state as for transition A ($^3B_2$) to the first excited state of Al_3, the D_{3h} $^2A_2''(^2B_1)$ state. This state is also accessed, from the Al_3^- ground state, in transition Y (Fig. 1). The CC adiabatic electron detachment energy for transition B is 1.739 eV, close to the measured 1.699 ± 0.004 eV value. In addition, the 211 cm^{-1} calculated bending frequency for the $^3B_2$ state agrees with the 202 ± 15 cm^{-1} anion bending frequency measured from the transition B hot band. This $(1b_1)^1(3a_1)^2(2b_2)^0 \leftarrow (1b_1)^2(3a_1)^1(2b_2)^1$ transition (us-

ing C_{2v} labels) would involve an electron detachment as well as an electron rearrangement, a factor that would account for its relatively weak observed intensity.

The top panel of Fig. 2 displays the Franck–Condon spectrum of the $^2A_2'' \leftarrow {}^3B_2$ transition calculated using the SRC method, with $\mathbf{K}''$ values for the symmetric stretching and bending normal mode displacements of −0.355 and 0.576 amu$^{1/2}$ Å, respectively. The bending intervals in the $^2A_2''$ state are noticeably underestimated in the simulated spectrum ($\nu_2' = 177$ cm^{-1}, calculated; 197 ± 10, observed), and the bending progression is slightly too intense. Adjustment of the calculated displacements to better match the spectrum, retaining the same normal mode vectors and assuming the calculated $^3B_2$ anion geometry, gives a $^2A_2''$ bond length of 2.592 Å and a bond angle of 60.6°, values differing only slightly from those calculated (2.603 Å, 60.0°). As noted above, for transition Y, comparison of the observed and simulated spectra (assuming the calculated Al$_3^-$ ground state geometry) would suggest a correction to the $^2A_2''$ Al$_3$ bond length of 0.01 Å in the opposite direction. These small discrepancies may reflect deviations of the observed vibronic band intensities from those expected based on the harmonic Franck–Condon model.

The Duschinsky rotation matrix for transition B is the same as for transition A ($J_{11} = J_{22} = 0.97$, $J_{12} = -J_{21} = -0.25$, Table III), which also accesses a D_{3h} Al$_3$ state from the C_{2v} $^3B_2$ anion. As shown in the lower panel of Fig. 2, use of the parallel mode Hutchisson method with $\mathbf{K}'$ displacements ($\Delta Q_1 = 0.201$, $\Delta Q_2 = -0.646$ amu$^{1/2}$ Å) gives a very similar spectrum (dashed line) to that obtained in the top panel with the SRC method with $\mathbf{K}''$ displacements, as was also observed for transition A. These $\mathbf{K}'$ displacements also agree, to within the estimated ±10% experimental uncertainties, with the magnitudes measured from fits to the spectrum in Paper I ($\Delta Q_1 = 0.20 \pm 0.02$, $\Delta Q_2 = -0.60 \pm 0.06$ amu$^{1/2}$ Å).

Particularly in view of the two-electron nature of the $^2A_2''(^2B_1) \leftarrow {}^3B_2$ assignment for transition B, alternative assignments warrant careful consideration. As shown in Fig. 3, the assignment of this transition as arising from the $^3A_2(1b_1)^1(3a_1)^2(2b_2)^1$ excited state of Al$_3^-$ and accessing the same $^2A_2''$ Al$_3$ state, which would be a one-electron process, gives a poorer match to the observed spectrum. In addition, the calculated detachment energy for the $^2A_2'' \leftarrow {}^3A_2$ transition of 1.539 eV is 0.16 eV lower than the measured value (1.699 ± 0.004 eV). The $^4A_2(1b_1)^1(3a_1)^1(2b_2)^1 \leftarrow {}^3A_2(1b_1)^1(3a_1)^2(2b_2)^1$ transition would also be a one-electron detachment process and has a calculated detachment energy of 1.615 eV, in better agreement with the observed energy of the transition B origin band. The simulated Franck–Condon spectrum for this transition is shown in the dashed spectrum at the top of Fig. 3, with its origin aligned with that of the higher-energy transition, C. This simulated transition shows a bending progression whose intensity is weaker than that observed in transition B, and the upper state 157 cm^{-1} bending intervals are also in poorer agreement with observed 197 ± 10 cm^{-1} intervals. The 202 ± 15 cm^{-1} anion bending frequency measured for transition B also differs significantly from the 165 cm^{-1} value calculated for the $^3A_2$ state. In addition, the assignment of transition B as aris-

ing from the $^3A_2$ anion would imply that the one-electron detachment from this anion state to the $^2A_2''(^2B_1)$ state of Al$_3$ would also be observed, with a calculated energy of 1.539 eV as noted above. This transition (shown in the dashed line in Fig. 3 with its origin aligned with that of transition B) would then overlap transition A. Although the $^2A_2'' \leftarrow {}^3A_2$ transition may contribute in this region, no clear evidence for it is detected. Finally, the agreement between the energy splittings measured (Table 1 of Paper I) for transitions X and Y (0.192 eV) versus A and B (0.191 eV) suggests that both sets of transitions access the same neutral molecule states and arise from the ground (X and Y) and a single excited (A and B) state of the anion. Thus, despite the necessity to invoke a two-electron detachment process, we conclude that transition B accesses the $^2A_2''$ state of Al$_3$ (as does transition Y) and arises from the $^3B_2$ state of Al$_3^-$ (as does A).

III.B.5. Transition C

A second one-electron photodetachment transition from the excited $^3B_2$ anion state that is expected to be observed in the 488 nm spectrum accesses the high-spin $^4A_2((1b_1)^1(3a_1)^1(2b_2)^1)$ state of Al$_3$ by detachment of an electron from the doubly occupied $1b_1$ orbital. The CC calculated adiabatic electron detachment energy for the $^4A_2 \leftarrow {}^3B_2$ transition is 1.815 eV, in excellent agreement with the value of 1.806 ± 0.004 eV measured for transition C. The calculated symmetric stretching frequency, ν_1', for the $^4A_2$ state (320 cm^{-1}) also agrees with the measured value for the Al$_3$ state accessed in this transition (315 ± 15 cm^{-1}), while the bending frequency, ν_2', is slightly overestimated (157 cm^{-1}, calculated; 140 ± 10 cm^{-1}, observed). The predicted spectrum for transition C is shown at the left of Fig. 2. The greater than observed intensity of the band due to the 1_0^1 and 2_0^2 transitions and of the higher-energy band results in part from the overestimated ν_2' frequency, which increases the overlap of different vibrational transitions in the simulated spectrum. As indicated in Table III, the calculated $\mathbf{K}'$ displacements (which are close in magnitude to the $\mathbf{K}''$ values since the off-diagonal $\mathbf{J}''$ matrix elements are small) are similar to those obtained in Paper I. The calculated increases in the bond lengths (0.072 Å) and bond angle (3.9°) in the $^4A_2 \leftarrow {}^3B_2$ transition also agree with the values (0.062 ± 0.013 Å and $3.9 \pm 1.0°$) deduced in Paper I from the normal mode displacements (assuming zero $^3B_2$ interaction force constants).

An alternative assignment of C as the $^4A_2 \leftarrow {}^3A_2$ transition, which would also be a one-electron detachment, can be rejected in view of the dissimilarities between the predicted and observed vibronic band intensity profiles, as shown in the top panel of Fig. 3. In addition, the corresponding calculated electron detachment energy (1.615 eV) differs substantially from the observed value (1.806 eV).

III.B.6. Transition D

The third one-electron transition from the $^3B_2$ excited state of Al$_3^-$ predicted to be observed in the 488 nm (2.540 eV) spectrum accesses the Al$_3$ $^2B_2$

$((1b_1)^2(3a_1)^0(2b_2)^1)$ state by detachment of the $3a_1$ electron. The CC detachment energy for this $^2B_2 \leftarrow {}^3B_2$ transition is 2.259 eV, only 2% higher than the measured 2.213 ± 0.006 eV value. The very similar bond lengths (2.504 Å $^3B_2$, 2.509 Å $^2B_2$) and bond angles (64.9°, 65.1°) calculated for these states indicate that detachment of the $3a_1$ electron produces little change in the equilibrium geometry, as is also predicted for transition X between the D_{3h} Al_3^- and Al_3 ground states for detachment from the same $2a_1'(3a_1)$ orbital. Thus, as shown in Fig. 1, the $^2B_2 \leftarrow {}^3B_2$ transition (short dashed lines) is predicted to display no detectable vibrational structure in ν_1 or ν_2 when added (long dashed lines) to overlapping transition Y. These predictions are in accord with the observed spectrum, from which only upper limits for ΔQ_1 and ΔQ_2 were reported for transition D based on the absence of observed vibrational structure.[35] Surprisingly, although the ν_1 and ν_2 frequencies have similar values in the $^3B_2$ and $^2B_2$ states, the calculated $^2B_2$ ν_3 frequency (382 cm^{-1}) is much higher than in the $^3B_2$ state (259 cm^{-1}). For the assumed ν_3 anion temperature (from Paper I) of 200 K for this spectrum of anions prepared in the short liquid nitrogen cooled flow tube, this anomalously large increase in the calculated ν_3 frequency produces a 3_1^1 sequence band to the left (blue) of the transition D origin in the simulated spectrum. The absence of this feature in the observed spectrum, as well as the large magnitude of the calculated $f(rr)$ interaction force constant (Table II), suggest that the PBE0 calculation overestimates the ν_3 frequency in the excited $^2B_2$ state of Al_3.

As noted in Paper I, the least squares fits to the origin band positions for transitions D and C gave essentially the same separation (0.407 ± 0.006 eV) as for transitions X and A (0.409 ± 0.004 eV). The corresponding energy splittings are calculated to be 0.395 and 0.444 eV, respectively (Table II), a difference of only 0.05 eV. As was previously surmised, the nearly perfect agreement between the two measured values appears to be coincidental.

The fourth one-electron transition from the $^3B_2$ excited state of Al_3^- that may potentially lie within the 2.54 eV window accessible in the 488 nm photoelectron spectrum involves the detachment of the other (β) electron from the doubly occupied $1b_1$ anion orbital, to produce a low-spin $^2A_2$ Al_3 state with unpaired α and β electrons. States of this type would be intrinsically multideterminantal[68] and are unlikely to be treated accurately by the density functional method employed here. The 488 nm photoelectron spectra do not display any clear evidence for this transition, whose vibronic band intensity profile is likely to be similar to that of transition C.

III.B.7. UV photodetachment transitions

The 193 nm UV photoelectron spectrum displays an additional band, labeled A', at 2.57 ± 0.08 eV electron binding energy (eBE),[36] which was also observed (there labeled Y) in the earlier 248 nm UV spectrum[37] but is just beyond the energy range of the vibrationally resolved 488 nm (2.540 eV) spectrum. This feature was originally assigned as a transition from the excited $[^3A_1]$ $((1b_1)^2(3a_1)^1(4a_1)^1)$ state of Al_3^- to the $^2A_1$ $((1b_1)^2(3a_1)^0(4a_1)^1)$ state of Al_3.[36] With

the present reassignment of the lowest stable Al_3^- excited state as the $^3B_2$ state, the corresponding assignment for the 2.57 eV band would be to the $^2B_2 \leftarrow {}^3B_2$ transition; however, this transition has already been assigned above to D at 2.213 eV. Subsequent computational studies suggested that the 2.57 eV feature is due to a transition (X1) from the Al_3^- ground state to this $^2B_2$ state.[5] According to the present calculations (Table I), the adiabatic electron detachment energy for this transition is 2.654 eV (CC), in agreement with the observed value. In addition, the two-electron nature of this transition would be consistent with the relatively weak observed intensity of the 2.57 eV band.[36,37] Two other Al_3 structures, the $(2)^2B_2$ $((1b_1)^0(3a_1)^2(2b_2)^1)$ and $[(2)^2A_1]$ $((1b_1)^0(3a_1)^2(4a_1)^1)$, have CC adiabatic detachment energies (from the Al_3^- ground state) of 2.88 eV, only 0.2 eV higher. Transitions to these structures from the Al_3^- ground state, which would also be two-electron processes, could contribute to this broad, asymmetric feature.[36,37]

However, the assignment of the 2.57 eV band as due entirely to transitions from the Al_3^- ground state is not consistent with the reported dependence of its relative intensity on the experimental conditions, which suggests that it arises, at least in part, from an excited Al_3^- state[36,37] or from an impurity anion.[37] Contributions to this feature from the excited $^3B_2$ $((1b_1)^2(3a_1)^1(2b_2)^1(4a_1)^0)$ anion state might include the transition to the D_{3h} $^4A_1'(^4B_2)$ $((1b_1)^0(3a_1)^1(2b_2)^1(4a_1)^1)$ state calculated to lie 1.079 eV above the Al_3 ground state. This $^4A_1'(^4B_2) \leftarrow {}^3B_2$ transition, which would also require a two-electron process, has a CC adiabatic photodetachment energy of 2.603 eV and would produce an extended vibrational progression due to the large difference between the equilibrium geometries of the two states (Table I). Other contributions to this broad feature might include the $^4A_2''((2)^4A_2) \leftarrow {}^3B_2$ two-electron process, calculated at the PBE0 level to be only 0.15 eV higher in energy.

Energies calculated for higher Al_3 excited states in Table I suggest that the next group of transitions from the Al_3^- ground state that would be observable in a UV photoelectron spectrum would occur near $\sim$4.3 eV eBE, accessing states $\sim$2.4 eV above the Al_3 ground state. Although lower-energy Al_3 states at 1.1–1.9 eV are listed in Table I, these are quartets, to which a transition from the singlet Al_3^- ground state would be spin forbidden. Transitions from the Al_3^- ground state to doublet states with two electrons in the $2e'$ orbital [which presumably lie at higher energies than the corresponding $^4A_1'(^4B_2)$ and $^4A_2''((2)^4A_2)$ quartet states listed] are also expected to be unobservable, as these would involve three-electron processes. The species predicted near $\sim$2.4 eV include two pairs of Jahn–Teller doublets, each with one electron in the degenerate D_{3h} $1e''$ $(2b_1,1a_2)$ orbital. (As noted in Sec. III.A, the $[^2B_1]$ saddle point could not be calculated using the PBE0 method.) These four structures are accessible from the Al_3^- anion by two-electron processes and may be observable in the UV spectrum, as suggested by the observation in the 488 nm spectrum of transition B, which also involves a two-electron process. The next higher-energy Al_3 state in Table I, a quartet D_{3h} state in which the $1e''$ orbital is doubly occupied, is predicted to lie 3.833 eV above

the Al$_3$ ground state. The corresponding doublet states, likely to lie even higher in energy, would require three-electron processes to be accessed from the singlet Al$_3^-$ ground state and thus are not expected to be observable.

The large differences in the equilibrium geometries calculated for the Al$_3^-$ ground state versus the ~2.4 eV Al$_3$ excited structures would be expected to produce extended vibrational progressions and to further increase the observed vertical electron detachment energies above their ~4.3 eV calculated adiabatic values. For example, for the transition from the D_{3h} $\widetilde{X}$ $^1A_1'$ Al$_3^-$ ground state to the excited C_{2v} $^2A_2$ state, the apex bond angle is calculated to increase by 28° and the identical bonds to lengthen by 0.22 Å (Table I), corresponding to very large normal mode displacements ($\mathbf{K}''$) of -2.67 amu$^{1/2}$ Å for the symmetric stretch and -3.89 amu$^{1/2}$ Å for the bend. Convoluting each vibrational transition with a 20 meV wide Gaussian line shape, assuming a vibrational temperature of 200 K, and using the SRC method, the simulated Franck–Condon spectrum (not shown) displays a 0.19 eV wide (full width at half maximum), structureless Gaussian profile whose intensity maximum is shifted 0.549 eV to higher eBE than the origin transition, whose intensity is calculated to be 10^{20} times weaker. (Use of the parallel mode Hutchisson method with the corresponding $\mathbf{K}'$ displacements, $\Delta Q_1 = 2.12$ and $\Delta Q_2 = 4.22$ amu$^{1/2}$ Å, gives essentially the same results, with a 0.19 wide band whose maximum is shifted up by 0.549 eV from the origin.) Adding this 0.55 eV shift between the vertical and adiabatic electron detachment energies to the 1.92 eV EA and the $^2A_2$ energy of 2.51 eV obtained in the PBE0 calculation gives an estimated vertical detachment energy of 4.98 eV for the $^2A_2 \leftarrow \widetilde{X}$ $^1A_1'(^1A_1)$ transition. While vibrational levels at these high energies are unlikely to conform to the harmonic oscillator model, this example illustrates that photodetachment transitions whose origin bands are calculated to lie in the ~4.3 eV region may actually be observed several tenths of an eV higher in energy.

In accord with these predictions, the 193 nm UV photoelectron spectrum of Al$_3$ displays no photodetachment transitions above the 2.57 eV band (A') discussed above, until about 4.3 eV.[36] In this vicinity, three photodetachment transitions assigned as arising from the Al$_3^-$ ground state are observed, with estimated adiabatic electron detachment energies reported as 4.28 ± 0.08 ("B"), 4.60 ± 0.08 ("C"), and 4.90 ± 0.08 eV ("D").[36] These transitions were originally assigned[36] as detachments from the mainly $3s$-derived $1e'$ and $1a_1'$ D_{3h} Al$_3^-$ orbitals. According to the latter assignment for the highest energy band at 4.9 eV, this transition would access a D_{3h} $^2A_1'$ $((1a_1')^1(1e')^4(1a'')^2(2a_1)^2)$ excited state lying 3.0 eV above the Al$_3$ ground state. The present DFT calculations cannot characterize this state, which would collapse to the $\widetilde{X}$ $^2A_1'$ ground state, and time dependent PBE0 calculations did not identify it among the excited states located within 3.4 eV of the Al$_3$ ground state. The appearance of transitions due to detachment of a $1e'$ electron in this region is supported by calculations which yield a vertical detachment energy of 4.52 or 4.66 eV for the D_{3h} $^2E'$

state,[1,3] which would Jahn–Teller distort to C_{2v} $^2A_1$ and $^2B_2$ structures. PBE0 results for the [$^2B_2$] structure are discussed in Sec. III.A.

For the 4.3 eV band B,[36] reported as C at 4.4 eV in the earlier UV study,[37] an alternative assignment has been suggested based on equation-of-motion CC calculations at the Al$_3$ ground state geometry.[5] This transition (X2) is to a $^2A_1'(^2A_1)$ $((1a_2'')^0(2a_1')^2(3a_1')^1)$ state with a calculated energy of 2.45 eV above the Al$_3$ ground state, giving a predicted photodetachment energy of 4.39 eV.[5] This $^2A_1'(^2A_1)$ state, which would require a two-electron process to be accessed from the Al$_3^-$ ground state, was not identified in the present PBE0 or time dependent PBE0 calculations. Time dependent B3LYP calculations have suggested that the 4.3 eV peak be assigned to an excited $^2E''$ $(1a_2'')^2(2a_1')^0(1e'')^1$ Al$_3$ state, whose vertical detachment energy was tentatively reported as 4.41 eV.[1] As discussed above, the present calculations find the corresponding C_{2v} Jahn–Teller pair of $(2)^2A_2$ and $[(2)^2B_1]$ structures to have adiabatic electron detachment energies near 4.35 eV at the CC level. Thus, these structures, as well as the nearby pair in which the $2a_1'(3a_1)$ rather than the $1a_2''(1b_1)$ orbital is doubly occupied, appear to provide possible assignments for the high energy transitions in the UV photoelectron spectrum.

III.C. Natural bond order analysis

Natural bond order (NBO) analysis[69] has been used to gain insight into the bonding in bare and partially ligated metal dimers.[70,71] NBO analyses were done in GAUSSIAN for the PBE0 calculated ground states of Al$_3$ and Al$_3^-$ at their D_{3h} equilibrium geometries. The 3CBOND keyword was activated to search for three-center bonds.

As is detailed in Table S-II in the Supporting Information,[61] the NBO description of the Al$_3^-$ $\widetilde{X}$ $^1A_1'(^1A_1)$ D_{3h} singlet ground state successfully identifies two three-center bonds and finds no two-center bonds. These results agree with the description of this $(1a_2'')^2(2a_1')^2$ singlet state as involving two two-electron bonds, one $\pi(1a_2'')$ and one $\sigma(2a_1')$, which are delocalized over the three equivalent atoms. The π-bonding MO is described as being composed essentially entirely (orbital coefficient of 0.99) of the out-of-plane $3p_z$ AOs. The in-plane bond is described as 84% p and 12% s in character.

The NBO analysis for the Al$_3$ $\widetilde{X}$ $^2A_1'(^2A_1)$ ground state also finds a two-electron, three-center out-of-plane bond, as well as a three-center in-plane bond with essentially the same description as for the anion (85% p, 9% s), but now occupied by only one (α) electron. This occupation of the two three-center orbitals is as expected based on the $(1a_2'')^2(2a_1')^1$ electron configuration. Surprisingly, however, three additional bonds are also identified for the β electrons. These include a three-center bond (occupancy 1.00 electron) involving the $3s$ orbital on one Al atom and the $3p_{x,y}$ orbitals on the other two atoms, as well as two two-center bonds (each ~50% s, ~50% p) between the latter two atoms (0.77 and 0.69 electrons). These results suggest the need for caution in interpreting NBO descriptions for bare, cyclic metal trimers. Qualitatively, however, they suggest that the detachment of a $2a_1'$

TABLE IV. Comparison of calculated to experimental dissociation energies (eV). Calculated total energies in hartrees (E_h) at the CCSD(T)/CBS//PBE0/MG3 level. EA, IE, and dissociation energy (D_0) values include PBE0/MG3 zero point energies (eV) of 0.0169 (Al_2), 0.0204 (Al_2^-), 0.0097 (Al_2^+), 0.0530 (Al_3), 0.0536 (Al_3^-) and 0.0353 (Al_3^+). Experimental values show the uncertainty in the last digit(s) in parentheses.

Ground state	CC (E_h)	Electron affinity (eV)[a]		Ionization energy (eV)[a]	
		CC	Expt.	CC	Expt.
Al (^2P)	−241.934 96	0.442	0.432 83 (5)	5.976	5.985 768 (3)
Al$^-$ (^3P)	−241.951 22				
Al$^+$ (^1S)	−241.715 35				
Al$_2$ ($^3\Pi_u$)[b]	−483.922 75	1.540	1.46 (6)	5.968	5.989 (2)
Al$_2^-$ ($^4\Sigma_g^-$)[c]	−483.979 49				
Al$_2^+$ ($^2\Sigma_g^+$)[c]	−483.703 18				
Al$_3$ ($^2A_1'$)	−725.946 70	1.919	1.916 (4)	6.558	6.5 (1)
Al$_3^-$ ($^1A_1'$)	−726.017 24				
Al$_3^+$ ($^3A_2''$)[c]	−725.705 04				

Dissociation process	CC D_0 (eV)	Expt.[d,e]	Expt.−Calc.[f]	Expt. 2001[d,g]	Expt.−Calc. 2001[f]
Al$_2$ → 2 Al	1.421	1.34 (6)[h]	−0.08 (6)		
Al$_2^-$ → Al+Al$^-$	2.519	2.37 (12)	−0.15 (12)		
Al$_2^+$ → Al+Al$^+$	1.429	1.34 (6)	−0.09 (6)		
ΔD_0 (Al$_3^-$−Al$_3$)[i]	1.477	1.483 (4)	0.006 (4)		
Al$_3$ → Al+Al$_2$	2.385	**2.403 (1)**[e]	0.018 (1)	2.703 (5)[g]	0.318 (5)
Al$_3$ → 3 Al[h]	3.806	**3.74 (6)**	−0.07 (6)	4.04 (7)	0.23 (6)
Al$_3^-$ → Al+Al$_2^-$	2.764	**2.86 (7)**	0.10 (7)	3.16 (7)	0.40 (7)
Al$_3^-$ → Al$^-$+Al$_2$	3.862	**3.886 (5)**	0.024 (5)	4.186 (9)	0.324 (9)
Al$_3^-$ → Al$^-$+2 Al	5.282	**5.23 (7)**	−0.05 (7)	5.53 (7)	0.25 (7)
Al$_3^+$ → Al+Al$_2^+$	1.795	**1.89 (10)**	0.10 (10)	2.19 (11)	0.40 (11)
Al$_3^+$ → Al$^+$+Al$_2$	1.803	**1.89 (10)**	0.09 (10)	2.19 (11)	0.38 (10)
Al$_3^+$ → Al$^+$+2 Al	3.224	**3.23 (16)**	0.01 (16)	3.53 (17)	0.30 (10)

[a]Experimental adiabatic EAs: Al (Ref. 74), Al$_2$ (Refs. 72 and 73), and Al$_3$ (Ref. 35). Experimental adiabatic IEs: Al (Ref. 75) and Al$_2$ (Ref. 76). The IE of Al$_3$ is listed as 6.5 ± 0.1 eV based on the lower and upper bounds of 6.42 and 6.5 eV (Ref. 42).

[b]Results for Al$_2$ at the PBE0/MG3 level (with experimental results from Ref. 43 in parentheses): $\widetilde{X}\,^3\Pi_u\ r_e$ 2.730 Å (2.7011 ± 0.0015), ω_e 273 cm^{-1} (285.8); $^3\Sigma_g^-\,r_e$ 2.477 Å (2.4665 ± 0.0024), ω_e 349 cm^{-1} (350.01). Al$_2$ CC $^3\Sigma_g^-$ energy above $\widetilde{X}\,^3\Pi_u$: 302 cm^{-1} (T_e), 340 cm^{-1} (T_0).

[c]Results for Al$_2^-$, Al$_2^+$, and Al$_3^+$ at the PBE0/MG3 level: Al$_2^-$ ($\widetilde{X}\,^4\Sigma_g^-$) r_e 2.555 Å, ω_e 329 cm^{-1}; Al$_2^+$ ($\widetilde{X}\,^2\Sigma_g^+$) r_e 3.252 Å, ω_e 156 cm^{-1} (experimental 178 ± 8 cm^{-1}, Ref. 76); and Al$_3^+$ ($\widetilde{X}\,^3A_2''$) D_{3h}, 2.673 Å, 272 cm^{-1} (ν_1), 148 cm^{-1} (ν_2, ν_3).

[d]Experimental dissociation energies (D_0, eV) of ions are obtained from the tabulated neutral molecule dissociation energies, EA, and IE values, as described in Sec. III.D.

[e]Experimental dissociation energies (D_0, eV) for Al$_3$, Al$_3^-$, and Al$_3^+$ using the 2.403 ± 0.001 eV value measured for Al$_3$ → Al$_2$+Al (Ref. 38). These values, in bold, are recommended here based on the reassignment (Sec. IV.A) of the initial Al$_3$ state in the R2PI spectrum as the ground state. Experimental atomization energies converted to D_e values, using the measured vibrational frequencies, are 3.80 ± 0.06 eV for Al$_3$ and 5.28 ± 0.07 eV for Al$_3^-$.

[f]Difference (eV) between the experimental D_0 value in the adjacent (left) column and the calculated D_0 value (column 2), with the experimental uncertainties in the last digit(s) in parentheses.

[g]Experimental dissociation energies (D_0, eV) using the 2001 revised Al$_3$ → Al$_2$+Al value (Ref. 39), which was increased from that in Ref. 38 by the Al$_3$ $^4A_2$ T_0 energy. Also see note (e).

[h]Experimental Al$_3$ atomization energy is obtained from the sum of the Al$_2$ D_0^0 (Ref. 43) and D_0(Al$_2$−Al) values.

[i]Difference (eV) between the Al$_3^-$ and Al$_3$ atomization energies, (Al$_3^-$ → 2Al+Al$^-$)−(Al$_3$ → 3Al), equal to EA(Al$_3$)−EA(Al).

bonding electron (primarily *p* in character) from Al$_3^-$ may be offset by an increased bonding participation of the 3s orbitals, an idea that is discussed further in Sec. IV.C.

III.D. Dissociation energies

Table IV summarizes the calculated bond dissociation energies, obtained at the CC level, and compares these results with the experimental values, which are also discussed in Sec. V.C of Paper I.[35] At the top left of the table, the calculated total energies are listed (in hartrees) without zero point contributions. For comparison with experiment, the calculated molecular EAs, ionization energies (IEs), and dissociation energies (D_0), given in eV, include the contribu-

tions of the PBE0 zero point energies listed at the top of Table IV. Experimental values show the uncertainty in the last digit(s) in parentheses. For the dimer, additional results for the ground ($\widetilde{X}\,^3\Pi_u$) and first excited ($^3\Sigma_g^-$) states of Al$_2$ and for the ($\widetilde{X}\,^4\Sigma_g^-$) Al$_2^-$ and ($\widetilde{X}\,^2\Sigma_g^+$) Al$_2^+$ ground states are given in notes (b) and (c). Similar results for Al$_2$ and/or its ions have been reported in numerous computational studies.[4–6,8,11,22,30]

For the $\widetilde{X}\,^2A_1'(^2A_1)$ ground state of Al$_3$, the dissociation energy to form three Al atoms in their ^2P ground state is calculated to be 3.806 eV. This atomization energy agrees with the results of previous *ab initio* studies,[4,5,22] including

one which used the same CC method (87.74 kcal/mol =3.805 eV).[4] As described in that paper, the addition of terms incorporating core-valence interactions (ΔE_{CV}) and relativistic effects (ΔE_{SR}) for Al$_3$ and Al, as well as a spin-orbit correction for the $^2P_{1/2}$ ground state of Al (ΔE_{SO}), were found to lower the calculated D_0 value by 0.047 eV (1.09 kcal/mol) to 3.758 eV (86.65 kcal/mol).[4]

As noted in Table IV, the calculated EAs agree well with experiment, and the difference between the Al$_3^-$ and Al$_3$ atomization energies, which is equal to that between the Al$_3$ and Al EA values, is also in good agreement (1.477 eV, calculated; 1.483 ± 0.004 eV, measured). The predicted dissociation energy of Al$_2$ ($D_0 = 1.421$ eV) is close to the measured value (1.34 ± 0.06 eV).[43] The calculated dissociation energy of Al$_2^-$ ($\tilde{X}\,^4\Sigma_g^-$) to form Al(^2P)+Al$^-$(^3P) is 2.519 eV, only slightly above the estimated error bar of the 2.37 ± 0.12 eV experimental value. The latter value is obtained using the following thermochemical cycle, and thus it depends on the Al$_2$ EA:

$$D_0(Al_2^- \rightarrow Al^- + Al) = D_0(Al - Al) - EA(Al) + EA(Al_2).$$

However, the CC calculated Al$_3$ atomization energy of 3.806 eV is 0.23 eV lower than the experimental value of 4.04 ± 0.07 eV obtained by adding the measured dissociation energy of Al$_2$ to the currently recommended $D_0(Al_2 - Al)$ value[39] of 2.703 ± 0.005 eV. (The latter is cited here rather than the 2.701 ± 0.005 eV published value,[39] which was based on our preliminary measurement of the experimental $^4A_2$ energy.) This 0.23 eV difference between the experimental and CC calculated bond energies is surprisingly large at this level of theory. Since the calculated and experimental[43] Al$_2$ dissociation energies are in reasonable agreement, the 0.23 eV discrepancy is evidently due mainly to the difference between the 2.385 eV calculated value for the $D_0(\tilde{X}\,^2A_1'\, Al_3 \rightarrow \tilde{X}\,^3\Pi_u\, Al_2 + {}^2P\, Al)$ dissociation energy and its currently recommended experimental value[39] of 2.703 ± 0.005 eV.

In contrast, the originally reported experimental value[38] of 2.403 ± 0.001 eV for the $D_0(Al_2 - Al)$ dissociation energy differs by only 0.018 eV from the calculated 2.385 eV value. Use of the former value gives an experimental Al$_3$ atomization energy of 3.74 ± 0.06 eV, also in much better agreement with the calculated value of 3.806 eV. This comparison also extends to the dissociation energies of the Al$_3^-$ anion, shown in the next three rows of Table IV. These experimental values are obtained from the Al$_3$ and Al$_2$ dissociation energies combined with the measured EAs of Al$_3$,[35] Al$_2$,[72,73] and Al (Ref. 74) using the following thermochemical cycles:

$$D_0(Al_3^- \rightarrow Al^- + 2Al) = D_0(Al_3 \rightarrow 3Al) - EA(Al)$$
$$+ EA(Al_3),$$

$$D_0(Al_3^- \rightarrow Al^- + Al_2) = D_0(Al_2 - Al) - EA(Al)$$
$$+ EA(Al_3),$$

$$D_0(Al_3^- \rightarrow Al + Al_2^-) = D_0(Al_2 - Al) - EA(Al_2)$$
$$+ EA(Al_3).$$

For example, the atomization energy of Al$_3^-$ to form Al$^-$+2Al is calculated to be 5.282 eV, consistent with the 5.23 ± 0.07 eV value based on the original $D_0(Al_2 - Al)$ result,[38] but 0.25 eV lower than the 5.53 ± 0.07 eV value implied by the revised[39] Al$_3$ dissociation energy.

Table IV also reports bond dissociation energies of the Al$_3^+$ cation, which is calculated to have a $D_{3h}\,^3A_2''(^3B_1)$ $((1a_2'')^1(2a_1')^1)$ ground state with a 2.673 Å bond length, about 0.17 Å longer than in the $D_{3h}\,^2A_1'(^2A_1)((1a_2'')^2(2a_1')^1)$ ground state of Al$_3$. The calculated cation atomization energy is 3.224 eV, about 0.6 eV lower than that of Al$_3$. These changes are in the expected directions for the loss of an electron from the strongly π-bonding $1a_2''(1b_1)$ orbital. The experimental Al$_3^+$ (and Al$_2^+$) bond dissociation energies in Table IV were obtained from those of Al$_3$ (and Al$_2$) combined with the measured IEs, using the following thermochemical cycles:

$$D_0(Al_3^+ \rightarrow Al^+ + 2Al) = D_0(Al_3 \rightarrow 3Al) + IE(Al)$$
$$- IE(Al_3),$$

$$D_0(Al_3^+ \rightarrow Al^+ + Al_2) = D_0(Al_2 - Al) + IE(Al) - IE(Al_3),$$

$$D_0(Al_3^+ \rightarrow Al + Al_2^+) = D_0(Al_2 - Al) + IE(Al_2)$$
$$- IE(Al_3),$$

$$D_0(Al_2^+ \rightarrow Al^+ + Al) = D_0(Al - Al) + IE(Al) - IE(Al_2).$$

For example, the experimental Al$_3^+$ atomization energy, which depends on the IE values of Al$_3$ (Ref. 42) and Al,[75] is 3.23 ± 0.16 eV assuming the 2.403 eV $D_0(Al_2 - Al)$ value[38] and 3.53 ± 0.17 eV assuming the 2.703 eV value.[39] The calculated 3.224 eV Al$_3^+$ atomization energy agrees with the former value but is 0.31 eV lower than the latter.

The Al$_3$ IE is predicted to be 6.558 eV, a result slightly larger than the bracketed experimental value, which has a lower bound of 6.42 eV and an upper bound of 6.5 eV.[42] Since the experimental IE values for Al (Ref. 75) and Al$_2$ (Ref. 76) and the EA measurements for Al (Ref. 74) and Al$_3$,[35] which have relatively small uncertainties, all agree with the calculated values to within 0.02 eV, it appears likely that the IE of Al$_3$ is also quite close to its 6.56 eV calculated value.

The discrepancies between the computational predictions and the experimental measurements for the dissociation energies of Al$_3$, Al$_3^-$, and Al$_3^+$ are discussed further in Sec. IV.A.

IV. DISCUSSION

The results in Sec. III confirm the spectroscopic assignments proposed in Paper I (Ref. 35) and in previous computational studies[1,3,5] for the photodetachment transitions observed in the vibrationally resolved 488 nm photoelectron spectrum of mass-selected Al$_3^-$. For the two states of Al$_3^-$ and four states of Al$_3$ observed in this spectrum, the com-

parisons between experiment and theory, summarized in Table II, further validate the abilities of these calculations to accurately predict the ground and excited state properties of Al_3 and Al_3^-. For the two states of Al_3^- and three states of Al_3 for which experimental measurements of the symmetric stretching and bending vibrational frequencies are available, seven of the ten calculated values agree with experiment to within 11 cm^{-1} and two of the remaining values agree to within 20 cm^{-1}. The calculated equilibrium geometries for the six observed states also agree, to within the estimated experimental uncertainties, with the geometry differences deduced from Franck–Condon fits to the vibronic band intensity profiles in the photoelectron spectrum. This consistency is also exhibited by the close similarities between the calculated and observed photodetachment transitions in Figs. 1 and 2. For the CC energy calculations, the calculated EA of Al_3, as well as the energies of the four observed excited states of Al_3 or Al_3^- relative to their respective ground states, all agree with the corresponding experimental results to within 0.03 eV (0.7 kcal/mol).

IV.A. Al_3 dissociation energy and reinterpretation of the R2PI spectrum

In view of these results, it is quite surprising that the bond dissociation energies of Al_3 and Al_3^- predicted here and elsewhere[4,5] using high-level wave function methods differ by as much as 0.4 eV from the currently recommended experimental values. These comparisons are tabulated in the rightmost column ("Expt.−Calc.") at the bottom of Table IV. To further investigate possible sources of these inconsistencies, we first describe the R2PI spectroscopic results upon which the experimental dissociation energies of Al_3 (and indirectly those of Al_3^- and Al_3^+ also listed in Table IV) are based.[38] We then suggest a reinterpretation of these spectroscopic results that implies dissociation energies more consistent with the computational predictions.

The R2PI study of Al_3 reported an excited state with observed vibrational levels $\geq 16\,610$ cm^{-1} (≤ 6020 Å) above the lower-energy (initial) electronic state detected, which was originally assumed to be the ground state.[38] An extended progression was detected in a mode with vibrational constants of $\omega_e = 273.2(+2.58n) \pm 0.6$ cm^{-1} and $\omega_e x_e = 1.29 \pm 0.05$ cm^{-1} in the upper state, where n is the vibrational quantum number in this state of the first observed band. Weaker features lying ~ 133 cm^{-1} to the low-energy side of 9 of the 11 observed members of this progression were assigned as vibrational hot bands, giving a fundamental frequency of 132.60 ± 0.85 cm^{-1} in the lower electronic state. Additional bands lying ~ 205 cm^{-1} to the high-energy side of seven of the members of the main progression were assigned to a second active vibrational mode having a frequency of 204.74 ± 0.94 cm^{-1} in the upper state.

The R2PI experiments also observed an apparent continuum absorption underlying the discrete band system at wavelengths below about 5400 Å ($\geq 18\,500$ cm^{-1}). For the vibrationally resolved transition, neither the original study[38] nor a subsequent, higher resolution (0.005 cm^{-1}) R2PI study[40] was able to resolve the rotational structure, implying

an upper limit of 1 ns for the lifetime (for the $v' = 1 + n$ level of the ~ 273 cm^{-1} mode) in the upper state.[40] It was concluded that this short lifetime is due to its rapid nonradiative decay into the dense manifold of states associated with the unstructured absorption.[38] On the other hand, in the $19\,300–19\,000$ cm^{-1} region, excitation into either this quasicontinuum, or into the overlapping discrete bands, required unusually long lifetimes of $24–35$ μs for relaxation back to the ground state, as measured by varying the delay between the excitation and subsequent ionization laser pulses.[38] It was postulated that the unstructured absorption is associated with a highly distorted, linear or nearly linear Al_3 excited state, whose poor Franck–Condon factors for relaxation back down to the D_{3h} ground state account for the microseconds-long delay.

The original R2PI study reported an upper limit for the Al_3 bond dissociation energy to form Al_2 and Al in their ground states as $D_0(Al_2-Al) = 19\,378 \pm 10$ cm^{-1} (2.403 ± 0.001 eV).[38] This measurement was based on the abrupt loss of the Al_3^+ parent ion signal at shorter wavelengths, indicating the onset of predissociation above this energy. Since both the continuous and the discrete transitions ceased to be observed at the same energy, indicating the same predissociation threshold, it was concluded that both absorptions arise from the same lower electronic state of Al_3.[38,39] This was assigned as the ground state in the original analysis, which reported the D_0 value as an upper limit in view of the possibility that this photodissociation might produce electronically excited Al_2 photofragments.[38] In a subsequent reanalysis of the spectrum, it was argued that the abrupt cutoff did indeed correspond to the thermochemical threshold, with no barrier to dissociation to the Al_2 ($\tilde{X}\,^3\Pi_u$) $+ Al(^2P)$ ground state fragments.[39] However, the initial state of Al_3 probed in the R2PI study was reassigned as the excited $^4A_2$ state rather than the ground state.[39] This new assignment took into account the 488 nm photoelectron data described in Paper I, which reports an energy of 0.300 ± 0.004 eV and a bending frequency of 140 ± 10 cm^{-1} for this quartet Al_3 excited state. It was noted that the $^4A_2$ frequency is consistent with the ~ 133 cm^{-1} hot band intervals in the R2PI spectrum, whereas the Al_3 ground state lacks a similar frequency.[39] With the reassignment of the initial state probed in the R2PI spectrum as the $^4A_2$ state, the photodissociation threshold was increased by the $^4A_2$ energy to give the currently recommended value for the $D_0(Al_2-Al)$ dissociation energy.[39]

Thus, the assignment of the ~ 133 cm^{-1} intervals in the R2PI spectrum as vibrational hot bands arising from the $v = 1$ bending vibrational level in the initial Al_3 electronic state was the key motivation for its reassignment as the $^4A_2$ state and for the consequent augmentation of the Al_3 dissociation energy by the ~ 0.3 eV energy of this excited state. Below, we argue that this vibronic band assignment scheme[38,39] is not consistent with the data, and we propose an alternative set of assignments. In this discussion, vibronic bands will again be labeled as $v_{v''}^{v'}$, where $v = 1$ for the symmetric stretch, $v = 2$ for the bend, and $v = 3$ for the asymmetric stretch; v'' is the vibrational quantum number of mode v in the initial

(lower) Al$_3$ state, and ν' is its quantum number in the final (upper) Al$_3$ state. Thus, for example, $1_0''2_1^0$ represents a transition from $\nu_1''=0$ (stretch) and $\nu_2''=1$ (bend) in the lower electronic state to $\nu_1'=m$ and $\nu_2'=0$ in the upper state (with $\nu_3''=\nu_3'=0$), and 1_0^m represents a transition from $\nu_1''=0$ to $\nu_1'=m$ (with zero quantum numbers for the other two modes in both states). Since the asymmetric stretch, ν_3, would not be active in a transition between C_{2v} and/or D_{3h} states, as noted earlier, we focus here on the symmetric stretching and bending modes.

One possible assignment, proposed in the original paper,[38] is that the 133 cm^{-1} intervals are sequence bands in the same mode that gives rise to the main progression, which was labeled ν_1 but was not specifically identified as the symmetric stretch or the bend. With this assignment, as given in Table I of that paper,[38] the band 133 cm^{-1} to the red of the 1_0^m is the 1_1^{m+1} sequence band, arising from $\nu_1''=1$ in the initial Al$_3$ state and accessing the next higher symmetric stretching level $(m+1)$ in the upper state. In this case, the identification of this interval as the bending mode in the $^4A_2$ state[39] implies that the mode associated with the main progression in $\sim$273 cm^{-1} intervals is also the bend. Thus, this assignment implies that of the two upper state frequencies reported, 273 cm^{-1} is the bending and 205 cm^{-1} is the symmetric stretching frequency. This would be a reversal of the usual ordering in which the symmetric stretch has a higher frequency than the bend, as is observed for all five vibrationally resolved states of Al$_3$ or Al$_3^-$ in the photoelectron spectrum (Table II). The reversed order can occur if the apex bond angle in the upper state is less than 60°, as is calculated for the four Jahn–Teller saddle point structures of Al$_3$ included in Table I. However, the observed vibrational activity is then not consistent with a transition from the $^4A_2$ state, which is calculated to have a short bond length of 2.58 Å and a bond angle of 69°. In a transition from the $^4A_2$ state to a state with an apex bond angle of $<$60°, not only the bending but also the symmetric stretching mode is expected to display strong activity. For example, for all of the calculated states in Table I in which the symmetric stretching frequency is lower than that of the bend, the length of the identical side bonds is calculated to be at least 2.72 Å. This large change from the $^4A_2$ bond length would produce an extended symmetric stretching progression. However, the R2PI spectrum shows an extended progression only in the 273 cm^{-1} mode. The progression in the 205 cm^{-1} mode is weak, with transitions observed only to the $\nu'=1$ upper state level.

Alternatively, one may consider a scheme in which the main progression is assigned as the symmetric stretch (1_0^m), the 205 cm^{-1} intervals as the upper state bending frequency, and the 133 cm^{-1} intervals as 2_1^0 hot bands in the bending mode of the initial $^4A_2$ state as suggested.[39] From a consideration of the harmonic Franck–Condon factors for these two transitions in the parallel mode approximation,[60] the intensity of the $1_0^m2_1^0$ hot band is expected to be equal to that of the $1_0^m2_0^1$ combination band multiplied by two terms. These are the Boltzmann factor for the $\nu_2''=1$ level (relative to that of the zero point level) in the initial electronic state (0.53 for a 133 cm^{-1} vibrational level at 300 K) and the ratio of vibrational frequencies in the upper and lower states[60]

$(\nu'/\nu''=1.54$ for $\nu_2'=205$ cm^{-1}, $\nu_2''=133$ cm^{-1}); the product of these two terms is 0.81. In the independent mode approximation, the Franck–Condon factors for different vibrational modes (ν_1 and ν_2) are simply multiplied together. Thus, for an assumed vibrational temperature of 300 K, the $1_0^m2_1^0$ hot band is expected to be about 80% as intense as the $1_0^m2_0^1$ combination "cold" band accessing the same upper state $\nu_1'=m$ level. At the lower limit of the estimated vibrational temperature range of 200–300 K,[38] this value would be reduced to about 60%. However, it is observed, particularly for the lower-energy transitions (e.g., $m=n+2$ and $n+3$) in the R2PI spectrum, that the bands 133 cm^{-1} to the low-energy side of the 1_0^m are *more* intense than the corresponding $1_0^m2_0^1$ combination bands.[38] These considerations argue against the assignment of the 133 cm^{-1} intervals as due to $1_0^m2_1^0$ hot bands.

We propose instead the following assignment scheme for the vibrationally resolved R2PI transition. The initial state is assigned as the Al$_3$ ground state, in agreement with the original assignment.[38] The main vibrational progression (1_0^m) is assigned as the symmetric stretch (ν_1), whose intervals give a vibrational frequency of 273 cm^{-1} for this mode in the excited state. The measured vibrational constants ($\omega_e'=273.17$ cm^{-1} and $\omega_e x_e'=1.29$ cm^{-1}) (Ref. [38]) correspond to a Morse potential dissociation energy estimate ($D_e=\omega_e^2/4\omega_e x_e$) of 1.79 eV for the symmetric stretch in the upper Al$_3$ state, about half of the calculated ground state atomization energy (Table IV).

As a test of this ground state assignment, one would predict sequence bands in the symmetric stretch (1_1^{m+1}) to appear to the red of the 1_0^{m+1} bands and to be spaced from them by the Al$_3$ ground state symmetric stretching fundamental frequency of 357 ± 10 cm^{-1}. The observation of these symmetric stretching sequence bands requires that the $\nu_1''=1$ level be sufficiently populated, and their intensities would vary with different cluster source conditions. Although these 1_1^{m+1} sequence band intervals are not observed in the original R2PI experiment, they do appear to be present in a subsequent, higher resolution spectrum.[40] This R2PI spectrum displays a weak, unassigned band 85 cm^{-1} to the red of the 1_0^{n+1} band of the main progression. Since the 1_0^{n+1} band is 267 cm^{-1} to the red of the 1_0^{n+2},[38] this weak band appears 352 cm^{-1} (85+267) to the red of the 1_0^{n+2} transition, consistent with its assignment as the 1_1^{n+3} sequence band. The R2PI spectrum[40] also displays a weak band 85 cm^{-1} to the red of the 1_0^{n+2}. Since the latter band is 265 cm^{-1} to the red of the 1_0^{n+3},[38] this weak band lies 350 cm^{-1} to the red of the 1_0^{n+3}, consistent with its assignment as the 1_1^{n+4} sequence band. If it is assumed that the experimental uncertainty for each of the two 85 cm^{-1} intervals is at least ±1 cm^{-1}, then the 352 and 350 cm^{-1} values represent two consistent measurements of the ground state symmetric stretching frequency, both of which agree with the 357 ± 10 cm^{-1} value measured from the photoelectron spectrum for the Al$_3$ ground state. The 352 and 350 cm^{-1} intervals do not agree, however, with the symmetric stretching frequencies of 315 ± 15 cm^{-1} measured for the first two Al$_3$ excited states, the $^2A_2''$ and $^4A_2$ states (or with their 320 cm^{-1} calculated frequencies). Thus, the two 85 cm^{-1} intervals in this R2PI spectrum (whose higher-

energy region was not reported)[40] provide strong evidence in support of the assignment of the initial Al_3 state probed in the R2PI spectrum as its $\widetilde{X}\,^2A_1'$ ground state.

The 133 cm^{-1} intervals to the red of the 1_0^m bands can then be assigned as $1_0^m2_1^1$ sequence bands in the bending mode. (The analogous assignment for the asymmetric stretching sequence bands is discussed below.) The 133 cm^{-1} value is found to be constant (to within ± 3 cm^{-1}) for the nine intervals observed, consistent with its assignment as arising from the $v_2''=1$ level of the lower state and accessing the same $v_1'=m$ upper state level as does the corresponding 1_0^m band. Since the Al_3 ground state bending frequency is measured to be 240 ± 10 cm^{-1} from the photoelectron spectrum, this 133 cm^{-1} spacing gives a low value of $240-133 =107\pm 10$ cm^{-1} for the fundamental frequency of the bending mode in the excited state, indicating a very flat bending potential. The absence of $1_0^m2_0^1$ combination bands 107 ± 10 cm^{-1} to the blue of the 1_0^m transitions, which would be expected in a transition between D_{3h} and C_{2v} states in which the equilibrium bond angles differ significantly, suggests that the bending displacement (ΔQ_2) is zero or nearly zero, and thus that the upper state shares the D_{3h} symmetry of the ground state. Therefore, the ν_3 (asymmetric stretching) frequency in the upper state would be degenerate with its ν_2 bending frequency, and the $1_0^m2_1^1$ and $1_0^m3_1^1$ sequence transitions would have the same energies. A similar vibronic band pattern of bending/asymmetric stretching sequence bands appearing to the red of each member of a symmetric stretching progression is also observed in the photoelectron spectrum (Fig. 1) for transition Y between the D_{3h} Al_3^- ground state and the D_{3h} Al_3 first excited state.

With this large change in the ν_2 and ν_3 frequencies from 240 ± 10 cm^{-1} in the D_{3h} Al_3 ground state to 107 ± 10 cm^{-1} in the D_{3h} excited state, one would expect to observe $\Delta v =2$ transitions. (The corresponding Franck–Condon factor for a mode having zero displacement is discussed in Sec. S-III.F of the Supporting Information.[61]) Thus, the 205 cm^{-1} intervals observed to the blue of the 1_0^m bands can be assigned as $1_0^m2_0^2$ and $1_0^m3_0^2$ combination bands. The seven observed $1_0^m(2,3)_0^2$ bands are all spaced by a constant interval of 205 ± 3 cm^{-1} from the 1_0^m bands,[38] again consistent with their assignment as accessing the same upper state symmetric stretching level. The assignment of the 205 cm^{-1} interval as due to the $v_2'=2\leftarrow v_2''=0$ (and $v_3'=2\leftarrow v_3''=0$) transitions then implies an upper state ν_2 (and ν_3) frequency of $205/2 =102.5$ cm^{-1} in the harmonic approximation. This value is consistent with the 107 ± 10 cm^{-1} frequency deduced above. More precisely, if the upper state ν_2 and ν_3 levels are assumed to be harmonic at these low vibrational levels, then adding half the reported 204.74 ± 0.94 cm^{-1} value[38] to the 132.60 ± 0.85 cm^{-1} sequence band interval implies fundamental ν_2 and ν_3 frequencies of 235.0 ± 1.3 cm^{-1} in the Al_3 ground state. This result is consistent with, and (assuming an harmonic upper state bending potential) more precise than, the 240 ± 10 cm^{-1} Al_3 ground state bending/asymmetric frequency measured from the lower resolution 488 nm photoelectron spectrum.

Figure 4 shows a Franck–Condon simulation of the vibrationally structured R2PI transition based on the proposed
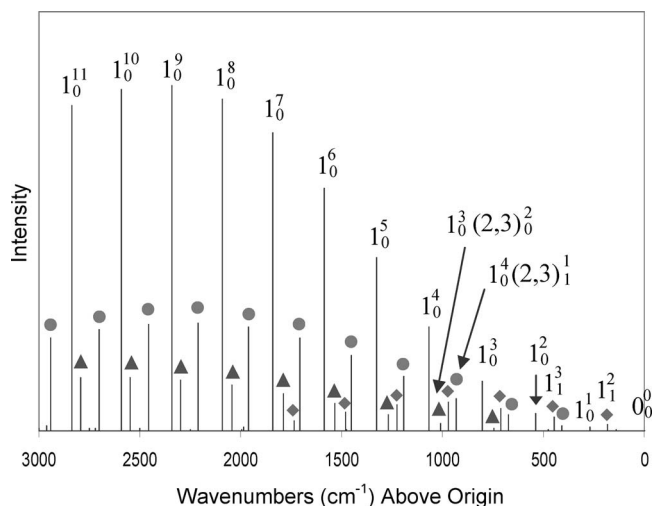

FIG. 4. Franck–Condon simulation of a transition from the D_{3h} $\widetilde{X}\,^2A_1'(^2A_1)$ Al_3 ground state to a D_{3h} excited state, with parameters chosen to model the R2PI spectrum (Ref. 38). Frequencies are ω_e'' 357 cm^{-1} for the symmetric stretch (ν_1) and 235 cm^{-1} for the degenerate bend and asymmetric stretch (ν_2,ν_3) in the ground state; for the excited state, $\omega_e'=273.17$ cm^{-1} and $\omega_e x_e'=1.29$ cm^{-1} for ν_1 and ω_e 102.37 cm^{-1} for ν_2 and ν_3. As in Fig. 1, the label 2_1^1 also represents the degenerate 3_1^1 transition (and 2_0^2 also represents 3_0^2) and stick heights are summed for degenerate transitions. Franck–Condon factors are calculated for Morse potentials for ν_1 (with $\omega_e x_e''\sim 0$), and for harmonic potentials for ν_2 and ν_3. A symmetric stretching displacement of $+1.30$ amu$^{1/2}$ Å and a ground state vibrational temperature of 200 K are assumed.

assignments, for a transition from the Al_3 ground state to a D_{3h} excited state. In view of the significant symmetric stretching anharmonicity in the upper state ($\omega_e x_e =1.29$ cm^{-1}),[38] Franck–Condon factors for the symmetric stretch are calculated for Morse oscillators by numerical integration of Laguerre wave functions, again using PESCAL.[52,55] Harmonic potentials are assumed for ν_2 and ν_3. For the assumed parameters as summarized in the figure caption, the simulated spectrum displays the major features of the observed R2PI spectra,[38,39] including the 1_0^m stretching progression, the $1_0^m(2,3)_1^1$ sequence bands 133 cm^{-1} to the red of the 1_0^m bands, the $1_0^m(2,3)_0^2$ combination bands 205 cm^{-1} to the blue of the 1_0^m bands, and the 1_1^{m+1} symmetric stretching sequence bands. Furthermore [with an exception of the $1_0^{n+1}(2,3)_1^1$ sequence band], this simulated Franck–Condon spectrum does not predict vibronic transitions of comparable intensities that are not observed. These results, which are discussed in greater detail in Sec. S-II of the Supporting Information,[61] provide additional support for the proposed assignments.

The equilibrium bond length of the Al_3 excited state in the vibrationally resolved R2PI transition cannot be determined by a Franck–Condon fit to the spectrum since the origin is not identified and the vibronic band intensities are uncorrected for the dye laser intensity.[38] Since the upper state symmetric stretching frequency (~ 273 cm^{-1}) is much lower than that of the ground state (357 ± 10 cm^{-1}), it is likely that the upper state bonds are longer (corresponding to a positive value of the symmetric stretching normal mode displacement). The simulation in Fig. 4 assumes a displacement of $+1.30$ amu$^{1/2}$ Å, which would correspond to a bond elonga-

tion (Δr) of 0.25 Å in the D_{3h} excited state [Eq. (6)]. Additional simulations discussed in the Supporting Information[61] suggest that the excited state bond length exceeds that of the ground state by at least 0.20 Å, providing an estimated lower limit of ≥ 2.71 Å for the excited state bond length.

This result is also sensitive to the use of anharmonic versus harmonic potentials in calculating the Franck–Condon factors. In Fig. 4, in which the symmetric stretching potentials are modeled by PESCAL as Morse oscillators,[52,55] the transition predicted to be most intense for the assumed $+1.30$ amu$^{1/2}$ Å symmetric stretching displacement is the 1_0^9, and the 1_0^{11} is more intense than the 1_0^7 by a factor of 1.1. In contrast, when the same parameters are used with the harmonic Hutchisson method,[60] the 1_0^{11} is predicted to be five times weaker than the 1_0^7 transition, which is the most intense in the progression. These results illustrate the large effects that even small vibrational anharmonicities (here, $\omega_e x_e = 1.29$ cm^{-1} in the upper state) can have upon the calculated Franck–Condon intensities.

With the initial state probed in the R2PI spectrum once again assigned as the Al$_3$ $\tilde{X}$ $^2A_1'$ ground state, the $D_0(\text{Al}_2-\text{Al})$ bond dissociation energy measurement of 2.403 ± 0.001 eV ($19\,378 \pm 10$ cm^{-1})[38,39] can be reinstated. The Al$_3$ and Al$_3^-$ bond dissociation energies based on this value are listed in boldface type in the last eight rows of Table IV. The column to their right lists the differences between these values (with experimental uncertainties in parentheses) and the energies calculated at the CC level. The calculated $D_0(\text{Al}_2-\text{Al})$ dissociation energy of 2.385 eV is now only 0.018 eV (0.7%) lower than the experimental value. The calculated Al$_3$ atomization energy of 3.806 eV falls essentially within the uncertainty of the measured 3.74 ± 0.06 eV value. For the ions, the calculated Al$_3^- \rightarrow 2\text{Al} + \text{Al}^-$ atomization energy of 5.282 eV also agrees with the measured value of 5.23 ± 0.07 eV, as does that of the Al$_3^+$ cation (3.224 eV, calculated; 3.23 ± 0.16 eV, experimental).

The R2PI spectrum provides several clues to the identity of the Al$_3$ excited state accessed in the vibrationally resolved transition. Since it is observed in a bound-bound optical transition from the doublet ground state, it can be assumed also to be a doublet state. In addition, if it is a D_{3h} state as suggested above, it is likely to have equal occupation of any doubly degenerate e' or e'' orbitals. Both of these considerations argue against the previously proposed $^4E'(^4A_1, {}^4B_2)$ quartet state assignment.[5] In the UV anion photoelectron spectrum, a transition from the Al$_3^-$ ground state to the R2PI excited state would appear (adding the 1.92 eV EA) at an electron detachment energy of 3.98 eV for the first observed 1_0^n band at 2.06 eV, and at 4.30 eV for the more intense 1_0^{n+10} band at 2.38 eV. The UV photoelectron spectrum does display a broad band at 4.30 eV. As discussed in Sec. III.B.7, however, a D_{3h} state at this energy, which is accessible from the Al$_3^-$ anion in a one- or two-electron process, was not identified in the present calculations.

One possibility for the D_{3h} excited R2PI state is one in which two degenerate orbitals are both singly occupied. Such a state would require a three-electron process to be accessed from the Al$_3^-$ ground state, so it would not be expected to be observed in the UV anion photoelectron spectrum. From the

Al$_3$ ground state, however, accessing this state would require a two-electron excitation (upon absorption of a single photon), a transition that might be observable. In the present photoelectron spectrum, weak transition B is firmly assigned as the $^2A_2''(^2B_1) \leftarrow {}^3B_2$ transition, which involves a two-electron process, and several such processes are discussed here and in previous studies[1,5] as possible assignments for some of the bands in the UV photoelectron spectra.[36,37] A doubly excited character might account for the weak intensity reported for the R2PI spectrum, which had been attributed to the low population of the excited $^4A_2$ state in the pulsed supersonic expansion when this was thought to be the initial state.[39] For the D_{3h} quartet $^4A_1'(^4B_2)$ $((1a_2'')^0(2a_1')^1(2e')^2)$ and $^4A_2''((2)^4A_2)$ $((1a_2'')^1(2a_1')^0(2e')^2)$ states in Table I, in which the two $2e'$ orbitals are both singly occupied, the calculated symmetric stretching frequencies are 237 and 282 cm^{-1}, respectively. The relatively high 273 cm^{-1} frequency in the upper R2PI state then suggests that its π-bonding $1a_2''$ orbital is singly occupied, as in the $^4A_2''$ state, rather than vacant, as in the $^4A_1'$ state. The $^4A_2''$ state is calculated to have a bond length of 2.74 Å, also consistent with the ≥ 2.71 Å value suggested above, and the corresponding doublet states may have similar geometries. As noted in Sec. III.A, the energy of this quartet state was not evaluated in the present CC calculations; its PBE0 calculated energy is 1.026 eV, and doublet states with nominally the same electron configuration would presumably lie higher in energy.

In summary, several clues regarding the identity of the excited state accessed in the vibrationally resolved R2PI transition are available. These include its spin multiplicity (doublet), geometry (D_{3h}, with estimated bond lengths of ≥ 2.71 Å), first (fundamental) and second (overtone) bending /asymmetric stretching vibrational levels (107 ± 10 cm^{-1}, 204.74 ± 0.94 cm^{-1}, when measured in combination with the observed symmetric stretching excitation in the upper state), its symmetric stretching frequency [$\omega_e = 273.2(+2.58n) \pm 0.6$ cm^{-1}, where n is the excited state vibrational quantum number of the first observed band at 16 610 cm^{-1}] and anharmonicity ($\omega_e x_e = 1.29 \pm 0.05$ cm^{-1}), and its energy (T_0) above the Al$_3$ ground state ($\leq 16\,610$ cm^{-1}, ≤ 2.06 eV).[38] As discussed in the Supporting Information,[61] the Franck–Condon simulation in Fig. 4 suggests that $n \geq 2$, reducing the latter value to $\leq 16\,060$ cm^{-1} (≤ 1.99 eV). Although a doublet state with three unpaired electrons cannot be characterized by the single determinantal density functional method employed here, it is suggested that a doubly excited $^2A_2''$ $(1a_2'')^1(2a_1')^0(2e')^2$ state may be a possible candidate.

IV.B. Validity of Franck–Condon simulation methods

In their introduction of the method (referred to here as the SRC method) to simulate Franck–Condon photoelectron spectra directly from the output of GAUSSIAN calculations, Chen and co-workers compared simulation methods with and without incorporation of Duschinsky rotation.[57] They concluded that the Franck–Condon factors are "wrong by an order of magnitude in the parallel mode approximation…. It

is clear that neglect of the Duschinsky rotation is the cause of serious error."[57] Thus, it is interesting that in the present study of the Al_3^- photoelectron spectrum, in which Franck–Condon analyses are performed using the programs FCFGAUS and PESCAL by Ervin, Lineberger, and co-workers,[52–55] such dramatic inconsistencies are not observed. As shown in Fig. 2, the analyses reported here employing the SRC method with $\mathbf{K}''$ normal mode displacements [Eqs. (2)–(5)] or the parallel mode approximation with $\mathbf{K}'$ displacements [Eqs. (7)–(9)] are found to provide mutually consistent results. This is true even for transitions A and B (Secs. III.B.3 and III.B.4) which, as indicated in Table III, have $\mathbf{J}''$ Duschinsky rotation matrices with significant off-diagonal elements. The compatibility of the two approaches is also evident in Table III, in which the normal mode displacements (ΔQ) obtained in Paper I by Franck–Condon fits to the spectra employing the parallel mode approximation are compared with $\mathbf{K}'$ displacements predicted from the PBE0 calculated geometries and vibrational properties.

As a further check on the consistency of these methods, Sec. S-III.H of the Supporting Information[61] provides a comparison of Franck–Condon simulations of the $CCl_2^+ \leftarrow CCl_2$ photoelectron spectrum that forms the basis for the conclusions quoted above.[56,57] As shown in Fig. S3(a) and S3(b),[61] it is found that for the originally reported GAUSSIAN 90 predictions,[56,57] the simulated Franck–Condon spectrum obtained using the parallel mode approximation (with $\mathbf{K}'$ displacements) displays an intensity maximum quite similar to that obtained using the SRC method (with $\mathbf{K}''$ displacements), consistent with the results obtained here for the $Al_3 \leftarrow Al_3^-$ photoelectron spectrum. We conclude therefore that the quoted conclusion is based on an erroneous calculation.

These results for the Al_3^- and CCl_2 photoelectron spectra support the observation[53,54] that calculated $\mathbf{K}'$ displacements are appropriate for use in combination with the parallel mode approximation when this method is preferred in order, for example, to compare predicted normal mode displacements with those reported in experimental studies assuming this approximation. Based on spectroscopic data, fitted normal mode displacements can be used to deduce the differences between the equilibrium geometries of the two electronic states, and these differences can be compared with those calculated, as is also done here. However, the deduction of geometry differences from Franck–Condon spectral intensities often requires assumptions concerning force constant values and the relative signs of different normal mode displacements, as discussed in Paper I. Thus, comparison of calculated $\mathbf{K}'$ displacements to measured normal mode displacements reported in experimental studies from Franck–Condon fits to the spectra in the parallel mode approximation can provide a more direct evaluation of the extent of agreement between theory and experiment. This common basis of comparison can be especially useful in studies of systems, such as clusters of open d-shell transition metals, for which accurate normal mode descriptions from spectroscopic or computational studies may not be available when the photoelectron (or other Franck–Condon) spectra are initially reported.

A further improvement in Franck–Condon spectral simu-

lation methods based on computational predictions is the incorporation of the effects of vibrational anharmonicities.[77–80] Anharmonic effects are not included in either the Hutchisson[60] or SRC[56–58] methods employed here. However, as is noted for the R2PI simulation in Sec. IV.A, Franck–Condon intensities can be quite sensitive to even small vibrational anharmonicities. The simulated CCl_2 photoelectron spectrum including estimated anharmonicities[81] in Fig. S3(d) of the Supporting Information[61] provides another example of this sensitivity. Thus, the effects of anharmonic vibrational potentials can be at least as important as those of Duschinsky mixing in achieving accurate comparisons between simulated and experimental spectra. Franck–Condon simulations incorporating both Duschinsky mixing and anharmonic effects have recently been reported for the anion photoelectron spectra of noncyclic triatomic molecules.[79,80] Although the present study of the cyclic aluminum trimer assumes harmonic potentials, it would be of interest to calculate the vibrationally resolved $Al_3 \leftarrow Al_3^-$ transitions using improved Franck–Condon simulation methods which incorporate both anharmonic and Duschinsky effects, particularly for transitions A-D which involve Jahn–Teller distorted Al_3^- and/or Al_3 states. To expedite comparisons of future computational predictions with experiment, the data displayed in Figs. 1–3 of the present paper are included in ASCII format in the Supporting Information for Paper I.[35]

IV.C. Ion-neutral total electron density difference distributions

In transition X (Sec. III.B.1) between the $\widetilde{X}\,^1A_1'(^1A_1)$ $((1a_2'')^2(2a_1')^2)$ Al_3^- and $\widetilde{X}\,^2A_1'(^2A_1)$ $((1a_2'')^2(2a_1')^1)$ ground states, both calculated to have D_{3h} symmetry, an electron is detached from the nondegenerate, totally symmetric $2a_1'(3a_1)$ HOMO. This orbital of the anion[2] involves mainly the in-phase combination of an in-plane $3p$ orbital on each atom, directed toward the center of the triangular cluster. Figure 5(a) depicts the square of this orbital, as calculated at the PBE0/MG3 level, showing isodensity contours in the molecular plane. The distribution of electron density in the internuclear regions is consistent with a bonding description for this orbital. This description is also in accord with the NBO analysis in Sec. III.C, which describes this as a three-center, two-electron bonding orbital which is primarily $3p$ in character. It is therefore surprising that the detachment of an electron from the $2a_1'$ Al_3^- orbital produces virtually no change in the equilibrium bond length or vibrational frequencies, as indicated by a comparison of these properties for the Al_3^- and Al_3 ground states in Table II. Transition D (Sec. III.B.6) between the excited $^3B_2$ and $^2B_2$ states of Al_3^- and Al_3 also involves detachment from this orbital and produces little change in the equilibrium geometry or in the ν_1 and ν_2 vibrational frequencies (Table II). Based on the negligible changes in bond distances and vibrational frequencies in these transitions, the $2a_1'$ Al_3^- orbital would be expected to be nonbonding.

In contrast, computational studies have emphasized the aromatic resonance stabilization afforded by the delocalized σ ($2a_1'$) as well as π ($1a_2''$) bonds in Al_3^-,[1–4,15] which are
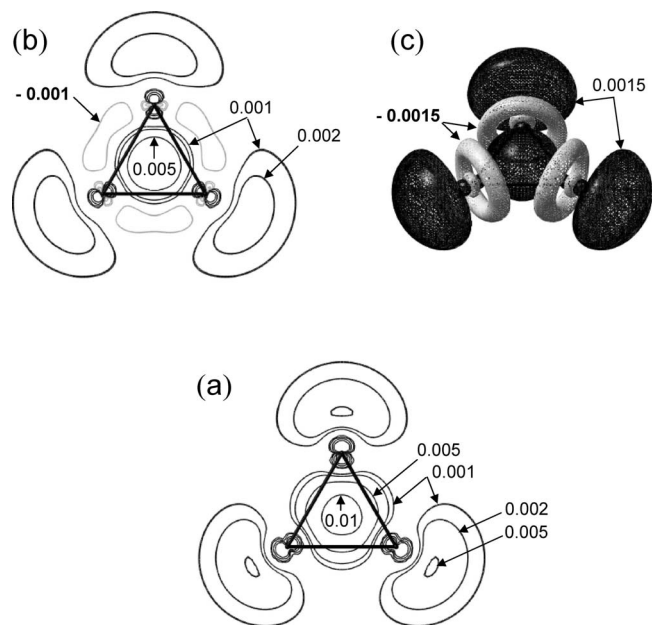
FIG. 5. (a) Square of the $2a_1'$ HOMO in the Al$_3^-$ $\widetilde{X}$ $^1A_1'$ ground state showing contours in the molecular plane for isodensity values of 0.001, 0.002, 0.005, and 0.010 e a_0^{-3}. (b) Total electron density difference plot (anion minus neutral) for transition X (Sec. III.B.1) between the $\widetilde{X}$ $^1A_1'$ Al$_3^-$ and $\widetilde{X}$ $^2A_1'$ Al$_3$ ground states, both calculated at the PBE0/MG3 level assuming the same D_{3h} geometry ($r=2.5071$ Å). Contours are shown in the molecular plane for the same isodensity magnitudes as in (a). Dark contours indicate decreased density in Al$_3$ as compared with Al$_3^-$, and light contours show regions of increased density in Al$_3$. (c) As in (b), but showing +0.0015 (dark) and −0.0015 e a_0^{-3} (light) isodensity surfaces with the molecule rotated by 45°.

estimated[4] to impart a total resonance energy stabilization in excess of 50 kcal/mol. In addition, the adiabatic electron detachment energy measured for Al$_3^-$ (1.916 ± 0.004 eV) (Ref. 35) considerably exceeds those of Al$_2^-$ (1.46 ± 0.06 eV)[72,73] or Al$^-$ (0.433 eV).[74] As noted in Sec. III.D, the difference between the Al$_3^-$ and Al$^-$ values also implies that the atomization energy of Al$_3^-$ (to form 2Al $+$Al$^-$) exceeds that of Al$_3$ by 1.483 ± 0.004 eV (34.2 ± 0.1 kcal/mol). In view of these considerations, the $2a_1'$ ($3a_1$) Al$_3^-$ anion HOMO can be considered to be bonding from an energetic standpoint. Thus, this orbital can be dualistically described as both energetically stabilizing and geometrically nonbonding.

Some insight into this apparent paradox may be gleaned from Fig. 5(b), which illustrates the difference between the total electron densities calculated for the Al$_3^-$ and Al$_3$ ground states, $\Delta(\psi^2)$. These results were obtained from single-point PBE0 calculations at the average (before rounding) bond length (2.5071 Å). As compared with a description in terms of a single MO from which the electron is detached, an **i**on-**n**eutral **t**otal **e**lectro**n de**nsity **d**ifference (INTEnDeD) distribution can offer a more authentic description of the changes in electronic structure accompanying electron detachment because it refers to a physical observable, the electron density. This difference includes orbital relaxation effects and is not restricted to a description of the electron detachment process in terms of Koopmans' approximation, which is notoriously poor for negative ions. A recent DFT study of changes in the bonding properties of transition metal complexes upon

oxidation also analyzed the electron density difference (for the neutral versus cationic species),[82] there referred to as the finite difference Fukui function.[83]

The total electron density difference plot in Fig. 5(b) displays isodensity contours in the molecular plane, for the same magnitudes as in Fig. 5(a) (0.010, 0.005, 0.002, and 0.001 e a_0^{-3}, where a_0 denotes a bohr), but includes negative values. In Fig. 5(b), the dark lines, labeled by positive isodensity values, represent regions of decreased electron density in Al$_3$ as compared to Al$_3^-$. As compared with the HOMO electron density plot in Fig. 5(a), the contours in Fig. 5(b) show a more modest loss of electron density in the internuclear regions upon electron detachment. In addition, as indicated in Fig. 5(b) by the light gray contours, there are also areas near the internuclear regions in which the electron density is calculated to *increase* upon electron detachment. This surprising aspect of the total electron density difference distribution is further illustrated in Fig. 5(c), which shows ±0.0015 e a_0^{-3} isodensity contours with the molecule rotated by 45°, with the light areas again representing regions of greater electron density in Al$_3$ than in Al$_3^-$. The gain in electron density near the Al–Al bonding regions upon electron detachment may reflect an increased participation in the bonding of orbitals of primarily 3s atomic parentage, as is qualitatively suggested by the NBO results described in Sec. III.C. These orbital relaxation effects may partially offset the loss of electron density in the bonding regions and contribute to the nonbonding character of the $2a_1'$ photodetachment transitions.

V. SUMMARY AND CONCLUSIONS

CCSD(T)/CBS//PBE0/MG3 calculations are reported for four electronic states of Al$_3^-$ and for 11 states of Al$_3$ (Table I). The results support the assignments of the six photodetachment transitions observed in the vibrationally resolved 488 nm photoelectron spectrum.[5,35] Calculations of the EA, the $^3B_2$ excited state energy of Al$_3^-$, the $^2A_2''(^2B_1)$, $^4A_2$, and $^2B_2$ excited state energies of Al$_3$, and the vibrational frequencies show good agreement with experiment (Tables II and III). These comparisons further validate the accuracy of these computational methods as applied to the ground and excited states of small Al clusters. Assignments for higher excited states of Al$_3$ observed in the UV photoelectron spectra[36,37] are also discussed. An NBO analysis of the Al$_3^-$ $\widetilde{X}$ $^1A_1'(^1A_1)$ ground state identifies two three-center, two-electron bonds as anticipated, but the NBO results for the Al$_3$ $\widetilde{X}$ $^2A_1'(^2A_1)$ ground state differ from the expected description.

A reinterpretation of the vibronic structure in the R2PI spectrum of Al$_3$[38,40] is proposed (Fig. 4), which supports the original[38] ground state assignment for the initial (lower) state probed in that experiment rather than the subsequent assignment to the excited $^4A_2$ state.[39] The structure in the vibrationally resolved transition is interpreted in terms of a progression in the symmetric stretch with the bending (and asymmetric stretching) modes having no normal mode displacements. These results suggest that the excited state accessed in the R2PI spectrum, like the ground state, has a D_{3h} geometry. Several possible clues to its identity are summa-

rized at the end of Sec. IV.A. The reassignment of the initial state probed in the R2PI spectrum as the Al_3 ground state reinstates the experimental D_0 (Al_2-Al) bond dissociation energy of 2.403 ± 0.001 eV. Other values that depend on this measurement are summarized at the bottom of Table IV in boldface type. With this revision, the experimental bond dissociation energies of Al_3, Al_3^-, and Al_3^+ are consistent with the computational predictions.

Geometry differences among the observed Al_3^- and Al_3 states, as obtained in Paper I from Franck–Condon fits to the experimental spectrum in the parallel mode approximation,[60] show good agreement with the calculated geometries (Table II). The simulated Franck–Condon spectra calculated using FCFGAUS and PESCAL[52–55] from the PBE0 equilibrium geometries and vibrational properties of the Al_3^- and Al_3 states using either the parallel mode method[60] (with $\mathbf{K}'$ normal mode displacements) or the SRC method[56–58] (with $\mathbf{K}''$ displacements) also agree well with the observed spectra. These results illustrate that use of the parallel mode approximation in interpretations of experimental photoelectron spectra, as is required for systems for which the information needed to characterize Duschinsky normal mode rotations is unavailable, can provide meaningful normal mode displacements and equilibrium geometry differences among the observed states. Of greater concern may be the assumption in both methods of the harmonic approximation (which, fortunately, appears adequate to model the photoelectron spectrum). For many systems, incorporation of vibrational anharmonicity as well as Duschinsky effects on Franck–Condon intensities based on computational studies is likely to be important in achieving good agreement with experiment.

The photodetachment transition between the Al_3^- and Al_3 ground states suggests that the $2a_1'(3a_1)$ HOMO of the anion can be described as nonbonding from the standpoint of its slight effects on geometrical and vibrational properties (Table II) but as bonding based on energetic criteria (Table IV). This dualistic character is further explored in Figs. 5(b) and 5(c) through the use of ion-neutral total electron density difference distributions, which depend on ψ^2, a physical observable. These plots reveal a region in which the electron density increases upon detachment of an electron from the $2a_1'$ anion HOMO, perhaps due to increased $3s$ contributions to the bonding. This orbital reorganization may partially offset the loss of bonding electron density and contribute to the nonbonding character of this photodetachment transition. These results for a well-characterized main group metal trimer, in which the $3p$ and $3s$ valence orbitals can contribute to the bonding, may find analogies in studies of the more computationally challenging, multiply bonded transition metal clusters, which can display both ns and $(n-1)d$ bonding contributions.

SUPPORTING INFORMATION AVAILABLE

Section S-I. CCSD(T) and PBE0 calculations: Further details concerning spin contamination and T_1 diagnostics (Table S-I) and NBO analyses (Table S-II).[61]

Section S-II. Al_3 R2PI spectrum: Additional discussion

of the simulated spectra and comparisons with the observed spectra (Figs. S1 and S2).[38,40]

Section S-III. Franck–Condon analysis methods: Comparison of the SRC and parallel mode methods and their consistency with those used Paper I.[35] Simulations of the CCl_2 photoelectron spectrum[56,57] (Fig. S3).

Section S-IV. References with full GAUSSIAN and MOLPRO citations (Refs. 44 and 49) and article titles.

Section S-V. Summaries of the calculated results used in Franck–Condon simulations (also provided in a text file): Al_3^- ($\tilde{X}\,^1A_1'$, $^3B_2$, $^3A_2$), Al_3 ($\tilde{X}\,^2A_1'$, $^2A_2''$, $^4A_2$, $^2B_2$), CCl_2, and CCl_2^+.[56,57]

ACKNOWLEDGMENTS

[1] A. I. Boldyrev and L.-S. Wang, Chem. Rev. (Washington, D.C.) **105**, 3716 (2005).
[2] A. E. Kuznetsov, A. I. Boldyrev, H.-J. Zhai, X. Li, and L.-S. Wang, J. Am. Chem. Soc. **124**, 11791 (2002); Figure 6, MO pictures.
[3] A. E. Kuznetsov and A. I. Boldyrev, Struct. Chem. **13**, 141 (2002).
[4] C.-G. Zhan, F. Zheng, and D. A. Dixon, J. Am. Chem. Soc. **124**, 14795 (2002).
[5] K. K. Baeck and R. J. Bartlett, J. Chem. Phys. **109**, 1334 (1998).
[6] D. E. Woon and T. H. Dunning, Jr., J. Chem. Phys. **101**, 8877 (1994).
[7] J. S. Tse, J. Chem. Phys. **92**, 2488 (1990).
[8] K. K. Sunil and K. D. Jordan, J. Phys. Chem. **92**, 2774 (1988).
[9] J. S. Tse, J. Mol. Struct. **165**, 21 (1988).
[10] G. Pacchioni, P. Fantucci, and J. Koutecky, Chem. Phys. Lett. **142**, 85 (1987).
[11] C. W. Bauschlicher, Jr., H. Partridge, S. R. Langhoff, P. R. Taylor, and S. P. Walch, J. Chem. Phys. **86**, 7007 (1987).
[12] H. Basch, Chem. Phys. Lett. **136**, 289 (1987).
[13] L. G. M. Pettersson, C. W. Bauschlicher, Jr., and T. Halicioglu, J. Chem. Phys. **87**, 2205 (1987).
[14] T. H. Upton, J. Chem. Phys. **86**, 7054 (1987).
[15] J. Sun, W. C. Lu, H. Wang, Z.-S. Li, and C.-C. Sun, J. Phys. Chem. A **110**, 2729 (2006).
[16] B. K. Rao and P. Jena, J. Chem. Phys. **111**, 1890 (1999).
[17] R. Ahlrichs and S. D. Elliott, Phys. Chem. Chem. Phys. **1**, 13 (1999).
[18] J. Akola, H. Häkkinen, and M. Manninen, Phys. Rev. B **58**, 3601 (1998).
[19] P. Calaminici, N. Russo, and M. Toscano, Z. Phys. D: At., Mol. Clusters **33**, 281 (1995).
[20] A. Martínez, A. Vela, and D. R. Salahub, J. Chem. Phys. **101**, 10677 (1994).
[21] R. O. Jones, J. Chem. Phys. **99**, 1194 (1993).
[22] N. E. Schultz, G. Staszewska, P. Staszewski, and D. G. Truhlar, J. Phys. Chem. B **108**, 4850 (2004).
[23] A. W. Jasper, P. Staszewski, G. Staszewska, N. E. Schultz, and D. G. Truhlar, J. Phys. Chem. B **108**, 8996 (2004).
[24] G. Staszewska, P. Staszewski, N. E. Schultz, and D. G. Truhlar, Phys. Rev. B **71**, 045423 (2005).
[25] N. E. Schultz, and D. G. Truhlar, J. Chem. Theory Comput. **1**, 41 (2005).
[26] A. W. Jasper, N. E. Schultz, and D. G. Truhlar, J. Phys. Chem. B **109**, 3915 (2005).
[27] D. Bhatt, A. W. Jasper, N. E. Schultz, J. I. Siepmann, and D. G. Truhlar, J. Am. Chem. Soc. **128**, 4224 (2006).
[28] D. Bhatt, N. E. Schultz, A. W. Jasper, J. I. Siepmann, and D. G. Truhlar, J. Phys. Chem. B **110**, 26135 (2006).
[29] A. W. Jasper, N. E. Schultz, and D. G. Truhlar, J. Chem. Theory Comput. **3**, 210 (2007).
[30] H. Li, D. Bhatt, N. E. Schultz, J. I. Siepmann, and D. G. Truhlar, J. Phys. Chem. C **111**, 16227 (2007).

[31] H. Li, A. W. Jasper, and D. G. Truhlar, J. Am. Chem. Soc. **129**, 14899 (2007).

[32] Z. H. Li and D. G. Truhlar, J. Phys. Chem. C **112**, 11109 (2008).

[33] N. E. Schultz, A. W. Jasper, D. Bhatt, J. I. Siepmann, and D. G. Truhlar, in *Multiscale Simulation Methods for Nanomaterials*, edited by R. B. Ross and S. Mohanty (Wiley-VCH, Hoboken, NJ, 2008), pp. 169–188.

[34] K. Park, D. Lee, A. Rai, D. Mukherjee, and M. R. Zachariah, J. Phys. Chem. B **109**, 7290 (2005).

[35] P. W. Villalta and D. G. Leopold, J. Chem. Phys. **130**, 024303 (2009).

[36] H. Wu, X. Li, X.-B. Wang, C.-F. Ding, and L.-S. Wang, J. Chem. Phys. **109**, 449 (1998).

[37] C.-Y. Cha, G. Ganteför, and W. Eberhardt, J. Chem. Phys. **100**, 995 (1994).

[38] Z. Fu, G. W. Lemire, Y. M. Hamrick, S. Taylor, J.-C. Shui, and M. D. Morse, J. Chem. Phys. **88**, 3524 (1988).

[39] Z. Fu, L. M. Russon, M. D. Morse, and P. B. Armentrout, Int. J. Mass. Spectrom. **204**, 143 (2001).

[40] B. Simard, S. A. Mitchell, D. M. Rayner, and D.-S. Yang, in *Metal-Ligand Interactions in Chemistry, Physics and Biology*, NATO Science Series, Series C: Mathematical and Physical Sciences Vol. 546, edited by N. Russo and D. R. Salahub (Kluwer, Dordrecht, 2000), pp. 245–248.

[41] S. Li, R. J. Van Zee, and W. Weltner, Jr., Chem. Phys. Lett. **262**, 298 (1996).

[42] D. M. Cox, D. J. Trevor, R. L. Whetten, and A. Kaldor, J. Phys. Chem. **92**, 421 (1988).

[43] Z. Fu, G. W. Lemire, G. A. Bishea, and M. D. Morse, J. Chem. Phys. **93**, 8420 (1990).

[44] GAUSSIAN 03, Revisions C.01 (for NBO 5.G) and D.01, M. J. Frisch, G. W. Trucks, H. B. Schlegel, *et al.*, Gaussian, Inc., Wallingford CT, 2004 (full citation given in Supporting Information).

[45] M. Ernzerhof and G. E. Scuseria, J. Chem. Phys. **110**, 5029 (1999).

[46] C. Adamo and V. Barone, J. Chem. Phys. **110**, 6158 (1999).

[47] A. D. McLean and G. S. Chandler, J. Chem. Phys. **72**, 5639 (1980).

[48] P. J. Knowles, C. Hampel, and H.-J. Werner, J. Chem. Phys. **99**, 5219 (1993).

[49] MOLPRO is a package of *ab initio* programs written by H.-J. Werner *et al.*, Versions 2002.6 and 2006.1 (full citation given in Supporting Information), see http://www.molpro.net.

[50] H.-J. Werner and P. J. Knowles, MOLPRO User's Manual Version 2006.1, University College, Cardiff Consultants Limited, 2006, Sec. 30.

[51] D. E. Woon and T. H. Dunning, J. Chem. Phys. **98**, 1358 (1993).

[52] K. M. Ervin, PESCAL (Versions 2004 and 2008) and FCFGAUS03, FORTRAN programs, http://wolfweb.unr.edu/~ervin/pes/.

[53] K. M. Ervin, T. M. Ramond, G. E. Davico, R. L. Schwartz, S. M. Casey, and W. C. Lineberger, J. Phys. Chem. A **105**, 10822 (2001).

[54] K. M. Ervin, J. Ho, and W. C. Lineberger, J. Phys. Chem. **92**, 5405 (1988).

[55] K. M. Ervin and W. C. Lineberger, in *Advances in Gas Phase Ion Chemistry*, edited by N. G. Adams and L. M. Babcock (JAI, Greenwich CT, 1992), Vol. 1, pp. 121–166.

[56] D. W. Kohn, E. S. J. Robles, C. F. Logan, and P. Chen, J. Phys. Chem. **97**, 4936 (1993).

[57] P. Chen, in *Unimolecular and Bimolecular Reaction Dynamics*, edited by C. Y. Ng, T. Baer and I. Powis (Wiley, Chichester, 1994), pp. 402–425.

[58] T. E. Sharp and H. M. Rosenstock, J. Chem. Phys. **41**, 3453 (1964).

[59] J. W. Ochterski, http://www.gaussian.com/g_whitepap/vib.htm.

[60] E. Hutchisson, Phys. Rev. **36**, 410 (1930).

[61] See EPAPS Document No. E-JCPSA6-129-002842 for the electronic supporting information summarized at the end of this paper. For more information on EPAPS, see http://www.aip.org/pubservs/epaps.html.

[62] E. B. Wilson, Jr., J. C. Decius, and P. C. Cross, *Molecular Vibrations* (Dover, New York, 1980; McGraw-Hill, 1955).

[63] T. C. Thompson, D. G. Truhlar, and C. A. Mead, J. Chem. Phys. **82**, 2392 (1985).

[64] E. Miyoshi, H. Tatewaki, and T. Nakamura, J. Chem. Phys. **78**, 815 (1983).

[65] I. Sioutis, V. L. Stakhursky, R. M. Pitzer, and T. A. Miller, J. Chem. Phys. **126**, 124308 (2007).

[66] N. Lambert, N. Kaltsoyannis, S. D. Price, J. Žabka, and Z. Herman, J. Phys. Chem. A **110**, 2898 (2006).

[67] J. C. Rienstra-Kiracofe, W. D. Allen, and H. F. Schaefer III, J. Phys. Chem. A **104**, 9823 (2000).

[68] C. C. Cramer, *Essentials of Computational Chemistry*, 2nd Ed. (Wiley, Chichester, 2004).

[69] E. D. Glendening, J. K. Badenhoop, A. E. Reed, J. E. Carpenter, J. A. Bohmann, C. M. Morales, and F. Weinhold, NBO 5.G, Theoretical Chemistry Institute, University of Wisconsin, Madison, WI, 2001, http://www.chem.wisc.edu/~nbo5.

[70] F. Weinhold and C. Landis, *Valency and Bonding: A Natural Bond Orbital Donor-Acceptor Perspective* (Cambridge University Press, Cambridge, 2005).

[71] G. L. Gutsev and C. W. Bauschlicher, Jr., J. Phys. Chem. A **107**, 4755 (2003).

[72] X. Li, H. Wu, X.-B. Wang, and L.-S. Wang, Phys. Rev. Lett. **81**, 1909 (1998).

[73] J. C. Rienstra-Kiracofe, G. S. Tschumper, and H. F. Schaefer III, Chem. Rev. (Washington, D.C.) **102**, 231 (2002).

[74] T. Andersen, H. K. Haugen, and H. Hotop, J. Phys. Chem. Ref. Data **28**, 1511 (1999).

[75] V. Kaufman and W. C. Martin, J. Phys. Chem. Ref. Data **20**, 775 (1991), http://physics.nist.gov/PhysRefData/Handbook/Tables/aluminumtable1.htm.

[76] J. E. Harrington and J. C. Weisshaar, J. Chem. Phys. **93**, 854 (1990).

[77] F. Chau, J. M. Dyke, E. P. Lee, and D. Wang, J. Electron Spectrosc. Relat. Phenom. **97**, 33 (1998).

[78] D. K. W. Mok, E. P. F. Lee, F. Chau, D. Wang, and J. M. Dyke, J. Chem. Phys. **113**, 5791 (2000).

[79] F. Chau, D. K. W. Mok, E. P. F. Lee, and J. M. Dyke, ChemPhysChem **6**, 2037 (2005).

[80] J. M. Dyke, E. P. F. Lee, D. K. W. Mok, and F. Chau, ChemPhysChem **6**, 2046 (2005).

[81] J. S. Guss, C. A. Richmond, K. Nauta, and S. H. Kable, Phys. Chem. Chem. Phys. **7**, 100 (2005).

[82] T. Leyssens, D. Peeters, A. G. Orpen, and J. N. Harvey, New J. Phys. **29**, 1424 (2005).

[83] P. Geerlings, F. De Proft, and W. Langenaeker, Chem. Rev. (Washington, D.C.) **103**, 1793 (2003).